

CONSORTIUM MATERIALS TECHNOLOGY for demonstration and development of thermal energy processes

FeCrAl alloys as components in biomass— and waste— fired boilers with sulphur additives

Kristina Hellström, Bonnie Hansson, Jan-Erik Svensson, Dilip Chandrasekaran, Bo Jönsson, Johanna Nockert-Olovsjö

KME-519



FeCrAl alloys as components in biomass- and waste- fired boilers with sulphur additives

Kristina Hellström Bonnie Hansson, Jan-Erik Svensson, Dilip Chandrasekaran, Bo Jönsson, Johanna Nockert-Olovsjö

Preface

The project has been performed within the framework the fifth stage of the material technology research programme KME.

KME, Consortium Materials technology for demonstration and development of thermal Energy processes, was established 1997 on the initiative of the Swedish Energy Agency. In the consortium, the Swedish Energy Agency, seven industrial companies and 18 energy companies participate. The programme stage has been financed with 60.2 % by participating industrial companies and with 39.8 % by Swedish Energy Agency. The consortium is managed by Elforsk.

The programme shall contribute to increasing knowledge to forward the development of thermal energy processes for various energy applications through improved expertise, refined methods and new tools. The programme shall through material technology and process technology developments contribute to making electricity production using thermal processes with renewable fuel more effective. This is achieved by

- Forward the industrial development of thermal processes through strengthen collaboration between industry, academy and institutes.
- Build new knowledge and strengthen existing knowledge base at academy and institutes
- Coordinate ongoing activities within academy, institutes and industry

KME's activities are characterised by long term industry relevant research and constitutes an important part of the effort to promote the development of new energy technology with the aim to create an economic, environmentally friendly and sustainable energy system.

Abstract

Kanthal® APMT, was investigated at 600 °C in 5 % O2 + 40 % H2O + 300 ppm SO2 with and without the presence of KCl. The mass gain was very low in the presence of SO_2 and was increased considerably in the presence of a combination of SO_2 and KCl. The added KCl was converted to stable K_2SO_4 . Chlorine was present at the point of initiation of the corrosion implying the existence of alloy chlorination. Pre-oxidation decreased the corrosion rate.

Sammanfattning

Kännetecknande för korrosion av överhettartuber i biomassa och avfall pannor är kombinationen av relativt låg metalltemperatur och en kemiskt aggressiv miljö. De material som konventionellt används i dessa kraftigt korrosiva applikationer är kromoxidbildande. Emellertid tenderar vissa kemiska reaktioner, i synnerhet bildning av alkali-kromat (VI), att utarma den skyddande oxiden på krom och omvandla oxiden till dåligt skyddande järnoxid vilket kan resultera i en plötslig ökning av korrosionshastigheten (breakaway korrosion). En möjlig strategi för att undvika de problem som skulle vara att använda en helt annan typ av material som bildar skyddande oxidfilmer som inte attackeras av temperaturområdet av intresse. En lösning skulle vara att aluminiumoxidbildande legeringar såsom de välkända FeCrAl stålen i dessa miljöer. Det känt också att korrosiviteten minskas vid införandet svavelhaltiga ämnen i pannan.

I detta projekt undersökte vi därför korrosionsbeteendet hos en aluminiumoxidbildande FeCrAl legering, Kanthal® APMT, vid 600 °C i 5% O_2 + 40% H_2O + 300 ppm SO_2 med och utan närvaro av KCl. Inverkan av föroxidering undersöktes också. Exponeringar utfördes i laboratorieugnar med en väl kontrollerad atmosfär. Kinetiken följdes med viktökningsmätningar. De bildade korrosionsprodukterna undersöktes med en rad analytiska instrument (XRD, SED/EDX, AES, IC och SIMS) för att utvärdera korrosions mekanismen.

Massökningen på Kanthal[®] APMT är mycket låg både i närvaro av SO₂ och utan SO₂. Massökningen är 20 gånger lägre än för 304L exponerad i närvaro av SO₂. Inledningsvis bildas en skiktad oxid med en inre aluminiumoxid, en kromoxid och en yttre Fe-rik oxid. Oxidationen fortgår genom diffusion av O²⁻ till oxid/metall gränssnittet och genom diffusion av Al³⁺ genom oxiden till oxid/gas gränssnittet. Det förefaller som att SO₂ hämmar tillväxten utåt av aluminiumoxiden. Exponering av materialet i närvaro av SO₂ och KCl ökar oxidationshastigheten avsevärt jämfört med en miljö utan KCl. Majoritetetn av den pålagda KCl omvandlas till stabil K₂SO₄. Cl var närvarande där korrosion börjat vilket antyder att legering klorineras. För-oxidation minskar korrosionshastigheten ännu mer. Dock flagar oxiden något vilket troligtvis är ett resultat av olika termisk expansion och/eller klorering av legeringen.

Alltså, den aluminiumoxidbildande FeCrAl legeringen Kanthal[®] APMT är inte helt inert mot KCl i en SO₂ innehållande oxiderande atmosfär vid 600°C. Dock är korrosionshastigheten signifikant lägre än för kromoxidbildande 304L. Föroxidering minskar korrosionshastigheten ytterligare vilket gör Kanthal[®] APMT till en lovande materialkandidat för komponenter i förbränningsanläggningar från en korrosion synvinkel.

Nyckelord: FeCrAl, aluminiumoxid, svaveldioxid, kaliumklorid

Summary

Characteristic for super heater corrosion in biomass and waste fired boilers is the combination of relatively low metal temperature and a chemically aggressive environment. The materials conventionally used in these severely corrosive applications are chromia-forming. However, certain chemical reactions, especially formation of alkali chromate (VI), that deplete the protective oxide in chromia tends to convert the oxide into poorly protective iron oxide and can result in a sudden increase in corrosion rate (breakaway corrosion). One possible strategy to avoid the problems would be to use a completely different type of materials that form protective oxide films not attacked by alkali at the temperature range of interest. One solution would be to use alumina-forming alloys such as the well-known FeCrAl steels in these environments. It also known that the corrosiveness of the environment is decreased when introducing sulphur-containing species in the boiler.

Hence, In this project the corrosion behavior of a alumina forming FeCrAl alloy, Kanthal APMT, was investigated at 600 °C in 5 % O_2 + 40 % H_2O + 300 ppm SO_2 with and without the presence of KCl. The influence of preoxidation was also examined. The exposures were performed in laboratory furnaces with a well-controlled atmosphere. The kinetics was followed using mass gain measurements. The formed corrosion product was examined by a range of analytical instruments (XRD, SED/EDX, AES, IC and SIMS) to evaluate the corrosion course of event.

The mass gain of Kanthal[®] APMT is very low both in the presence of SO₂ and without SO₂. The mass gain is 20 times lower compared to 304L after exposure in the presence of SO₂. Initially a layered oxide forms with an inner alumina, a middle chromia and an outer Fe-rich oxide. The oxidation appears to proceed by inward diffusion of O²⁻ to the oxide/metal interface a by outward diffusion of Al³⁺ to the oxide/gas interface. SO₂ appears to inhibit the outward growth of the alumina scale. S enrichments are found on the surface and in the oxide scale, situated between the alumina scale and the Cr enrichment. Exposing the material in the presence of SO₂ and KCl increases the oxidation rate considerably compared to an environment without KCI. More than half of the applied KCl is converted to stable K₂SO₄ on the material surface during exposure. Cl was present where corrosion had started implying alloy chlorination. Pre-oxidation decreases the corrosion rate even further. However some spallation has occurred, likely as a result of thermal expansion miss match and/or alloy chlorination. After spallation the alumina scale is likely not re-healed due to the low Al diffusion rate at the exposure temperature.

Hence, the alumina forming FeCrAl material Kanthal APMT is not completely inert to KCl in an oxidizing SO_2 containing atmosphere at 600°C. However, the corrosion rate is significantly lower than for the chromia forming 304L. Pre-oxidation decreases the corrosion rate even further, making Kanthal APMT a promising candidate material for combustion plant components from a corrosion point of view.

Keywords: FeCrAl alloys, alumina, sulphur dioxide, potassium chloride

Table of contents

1	Intr	oductio		1
	1.1	Backgr	round	1
	1.2	Descri	ption of the research field	1
	1.3	Resear	rch task	2
	1.4	Goal		4
	1.5	Project	t organisation	4
2	Mate	erial		5
3	Expe	eriment	tal conditions	7
_	3.1	Materi	al preparation	
	3.2		ure equipment	
	3.3		ative corrosion analysis of exposed material	
		3.3.1	Gravimetric analysis	
		3.3.2	X-ray diffraction (XRD)	
		3.3.3	Scanning electron microscopy (SEM)	
		3.3.4	Broad ion beam (BIB)	
		3.3.5	Auger electron spectroscopy (AES)	
		3.3.6	Ion chromatography (IC)	
		3.3.7	Secondary ion mass spectrometry (SIMS)	
			, (,	
4	Resi	ults		11
	4.1	The ef	fect of SO ₂ in the presence of H ₂ O	11
		4.1.1	Macro appearance	11
		4.1.2	Mass gain	11
		4.1.3	Crystalline oxide products	13
		4.1.4	SEM/EDX	13
		4.1.5	Elemental depth profiles	16
		4.1.6	Water-soluble oxide products	
	4.2	The ef	fect of SO ₂ in the presence of KCI	21
		4.2.1	Macro apperance	21
		4.2.2	Mass gains	22
		4.2.3	Crystalline oxide products	
		4.2.4	SEM/EDX	
		4.2.5	Water-soluble oxide products	
	4.3		fect pre-oxidation in the presence of SO_2 and KCl	
		4.3.1	Macro apperance	
		4.3.2	Mass gain	
		4.3.3	Crystalline oxide products	
		4.3.4	SEM/EDX	33
		4.3.5	Water soluble oxide products	35
5	Δna	lysis of	the results	37
<u> </u>	5.1	. y3:3 01 S∩₂		
	5.2	SO₂ ar	nd KCI	38
	5.3	The ef	fect of pre-oxidation in the presence of SO_2 and KCl	40
_	_			. =
6	Con	clusion	S	42
7	Goa	l fulfilm	nent	44
8	Suga	aestion	s for future research work	45
J	Juu	46361011	is for facult i escalcii WUIK	+⊃

9	Literature references	46
10	Publications	48

1 Introduction

1.1 Background

For Sweden to be able to develop a sustainable energy system several high temperature corrosion problems must be solved. Corrosion problems in biomass or waste-fired combustion plants are important issues in this context. New more corrosion-resistant materials could mean less maintenance, less downtime, higher steam data, increased electrical output, etc.

This project investigates whether some components in biomass and waste-fired combustion plants can be replaced with more corrosion-resistant, FeCrAl materials. Laboratory exposures of FeCrAl materials will be performed using an environment mimicking the environment in biomass- and waste fired boilers where sulfur is added to decrease corrosion. We will examine the corrosion properties of commercial FeCrAl materials in these types of environments, which will provide a better understanding of the corrosion process in these environments and hence hint on how/where the material can be used. This could enable new designs of biomass-and waste-fired combustion facilities that make this important source of sustainable energy more competitive.

1.2 Description of the research field

Characteristic of corrosion in biomass-and waste-fired boilers is the combination of relatively low metal temperatures and a chemically aggressive environment. The materials conventionally used in these highly corrosive applications are mainly chromium oxide forming material. Recent work within the HTC has shown that certain chemical reactions, especially the formation of alkali chromate (VI), which depletes the protective oxide in chromium oxide tends to transform to poorly protective iron oxide which can lead to a sudden increase in the corrosion rate (break away corrosion). We have primarily worked with two novel reactions that can achieve this effect, evaporation of chromic acid and the formation of alkali chromate.

$$1/2Cr_2O_3(s) + 3/4O_2(g) + H_2O(g) \rightarrow CrO_2(OH)_2(g)$$

 $1/2Cr_2O_3(s) + 3/4O_2(g) + H_2O(g) + 2KCl(s) \rightarrow K_2CrO_4(s) + 2HCl(g)$

Both reactions deplete the protective oxide in chromium, which makes it difficult for the alloy to retain its corrosion resistance. Chlorine is another factor that also tends to accelerate corrosion of these materials, especially in waste-fired plants. Once the protective oxide has been destroyed, for example by alkali salts forming alkali chromate, the oxide is easily penetrated by chloride ions which lead to more serious corrosion.

A possible strategy to avoid the problem would be to use a completely different type of material that forms a protective oxide layer which is not attacked by alkali. One option would be to use alumina-forming alloys, such as the familiar FeCrAl steels, in these environments. FeCrAl alloys are primarily used at very high temperatures 900-1300°C, for example as heating elements in industrial furnaces. FeCrAl alloys are ferritic iron-based steel with a typical concentration of 18-25 weight% chromium and \sim 5 wt% aluminum. In addition, small amounts of reactive elements are added (yttrium, zirconium and hafnium) to enhance corrosion resistance and to improve the mechanical properties. The benefits of the group FeCrAl alloys are based on the formation of a slow-growing and very protective a-Al₂O₃ layer. However, the usefulness of aluminum oxide formers can be questioned at low temperatures (<900°C). This is because the alloy does not form a protective alumina-corundum-type oxide at low temperatures. The metastable aluminum oxides formed at lower temperatures have less protective properties than a-Al₂O₃. However the protective properties of the metastable aluminum oxides may still be superior to Cr₂O₃. Preliminary results indicate that a corundum type oxide containing aluminum, iron and chromium oxide is formed on FeCrAl materials at 600°C in an oxidizing atmosphere. The protective property of this oxide is not well known and may also be superior to chromia. The results from KME 414 hinted in that direction.

The corrosion rate of FeCr steels is known to decrease significantly by the addition of sulfur. Sulfur addition may also decrease the corrosion rate of FeCrAl alloys, possibly to the extent that a protective surface layer can stay intact.

1.3 Research task

This project can be seen as a continuation of KME 414 and KME 507. In KME 414 we investigated the possibility to use FeCrAl materials as super heaters in biomass- and waste- fired boilers at 600°C. The laboratory studies showed that KCl accelerates the corrosion of the two FeCrAl alloys Kanthal® AF and Kanthal® APMT in a similar manner as has been shown earlier in the case of chromium oxide forming high temperature steel. This is because the exposure temperature is too low for the two alloys to form a protective aluminum oxide layer. Instead, a mixed (Fe, Cr, Al) oxide is formed that reacts with KCl, O2 and H₂O forming potassium chromate during oxidation. The resulting chromium depleted oxide is poorly protective. In the field corrosion exposure, alloy APMT showed by far the best ability to resist corrosion. Both the "conventional" FeCrAl alloy Kanthal® AF and the chromium oxide forming 304L show metal losses of approximately twice that of APMT. Pre-oxidation of the samples had a positive effect on the ability of FeCrAl APMT alloy to resist KCl induced corrosion in relatively mild conditions in the laboratory exposures. In contrast, pre-oxidation had no positive effect on the corrosion behavior in the environment of the fire side in the waste-fired boiler. The difference between the effects of oxidation in the two cases is assigned provisionally to the differences in the corrosive environment.

In the KME 507, we (among other things) investigate why field and laboratory exposures differed from each other in KME 414. This is done through tougher laboratory tests with cycling and a higher amount of KCl. The addition of

sulfur has been shown earlier to significantly decrease the oxidation of low alloyed Cr-steels. In this project we want to extend the laboratory investigations to environments containing SO_2+H_2O and $SO_2+KCI+H_2O$ to investigate the effect that sulfur addition in the combustion plant would have on FeCrAl components. This will give new information needed for the understanding of the corrosion process of FeCrAl materials in combustion plants. The work will be focused on identifying mechanisms behind the corrosion and to find ways to alleviate the high temperature corrosion problems.

The material that will be exposed is the FeCrAl alloy Kanthal[®] APMT and the results will be compared with chromia forming materials already investigated at HTC.

The following scientific issues will be highlighted:

- What is the nature of the oxides formed at 600 in an oxidizing environment?
- How is the oxide formation affected by the presence of water vapor and sulfur dioxide?
- How is the oxide formation affected by the presence of small amounts of alkali compounds (KCI) in an atmosphere of water vapor and sulfur dioxide?
- Can the corrosive effect of alkali salts be mitigated by pre-oxidation in an atmosphere of water vapor and sulfur dioxide?

Laboratory study

The laboratory exposures will be conducted in a synthetic environment that mimics the corrosive environment in real boilers. The exposures will be performed on naked material or pre-oxidisedized material. We will examine:

- i. Influence of SO₂ and H₂O
 - a. The effect of water vapor and sulphurdioxide on the oxidation of Kanthal APMT will be studied in an oxygen containing environment at 600°C.
- ii. Influence of SO₂, H₂O and KCl.
 - a. Kanthal APMT will be exposed to KCl in a gas environment containing SO_2 , O_2 and H_2O . The research focus on the initial corrosion attack (<168 timmar).
- iii. Influence of pre-oxidation in the presence of KCl, SO₂ and H₂O
 - a. Kanthal APMT is pre-oxidized to form a protective aluminum and is thereafter exposed to KCl in a gas environment containing SO_2 , O_2 and H_2O .

Evaluation of the exposed samples

After exposure the material will be characterized by several different techniques. This includes X-ray diffraction (XRD), scanning electron microscopy (SEM/EDX), auger electron spectroscopy (AES), secondary ion mass spectrometry (SIMS) and focused ion beam microscopy (FIB). Together

these techniques will give us a thorough understanding of the formed oxide and the oxidation process.

1.4 Goal

The aim of this project will be to identify and understand the usability and the limitations of alumina forming materials as components in biomass- and waste fired combustion plant. In particular we will investigate the possible beneficial effect of sulphur additions on the corrosion of alumina forming alloys. The project is carried out in close collaboration with KME project 507. The work will be focused on identifying mechanisms behind the corrosion and to find ways to alleviate the high temperature corrosion problems. The project will include exposures of the material in complex well-controlled laboratory environments. The project will combine a number of analysis methods which will give us a thorough understanding of the formed oxide and the oxidation process.

1.5 Project organisation

The personnel at HTC (Chalmers) involved in the project and the following people at the industrial partners has participated in the project:

Kristina Hellström, HTC Bonnie Hansson, HTC Jan-Erik Svensson, HTC Dilip Chandrasekaran, Sandvik Heating Technology Bo Jönsson, Sandvik Heating Technology Johanna Nockert, Sandvik Heating Technology

The work within the project was divided between the project participants.

- The material studied was manufactured and supplied by Sandvik.
- The material was for prepared for exposure and exposed at Chalmers.
- The material was analyzed at Chalmers.
- HTC led the project.

The budget for the project was: HTC 767 kkr (financed through KME) and Sandvik 1162 kkr (in kind), in total 1929 kkr for a period of 1.25 years.

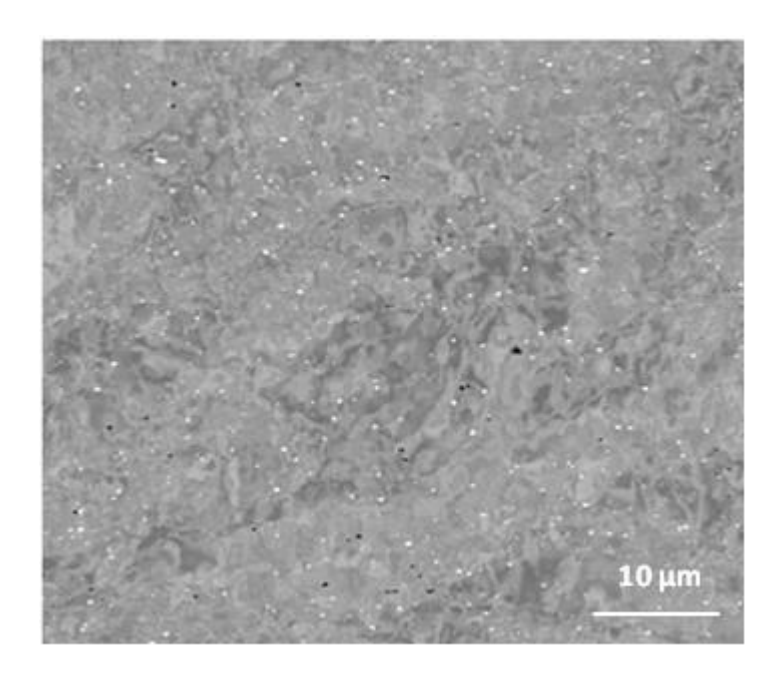
2 Material

The investigated material was Kanthal® APMT, which is an advanced, powder metallurgic commercially available ferritic iron-chromium-aluminum alloy (FeCrAl alloy). Kanthal® APMT is a Rapidly Solidified Powder (RPS) material composed of rare earth (RE) oxide particles dispersed in a FeCrAlMo matrix. The chemical composition is given in Table 1. The material is manufactured by hot isostatic pressing (HIP) of gas-atomized FeCrAlMo powder and oxidized RE particles at high temperatures (around 1150°C) in inert gas/vacuum.

The RE-rich particles appear as bright spots in Figure 1(a), with the size distribution ranging from ≤ 100 nm to about 0.5 µm. EDX analyses showed that the larger RE particles were more frequently rich in Y than the smaller RE particles, which were rich in Hf and Zr. Furthermore, while Ti was detected infrequently, it was always associated with other RE elements. The dark dots were frequently rich in Mg and/or O and sometimes N, always with a contribution from the matrix, i.e., Al, Cr, and Fe. Figure 1(b) shows a backscattered electron image of a finely polished and slightly etched surface of the unexposed APMT material. The grains, which appear to have an elongated structure with a width of approximately 1 µm, vary in length from 1 - 8 µm. Figure 1(c) shows a backscattered electron image of a polished, slightly etched APMT material that was exposed to 1100°C for 24 h. The grains have grown during the exposure time to approximately 10 – 20 µm. This is the stable grain size, meaning that the grain size will remain unchanged upon further exposure to the high temperature 1 .

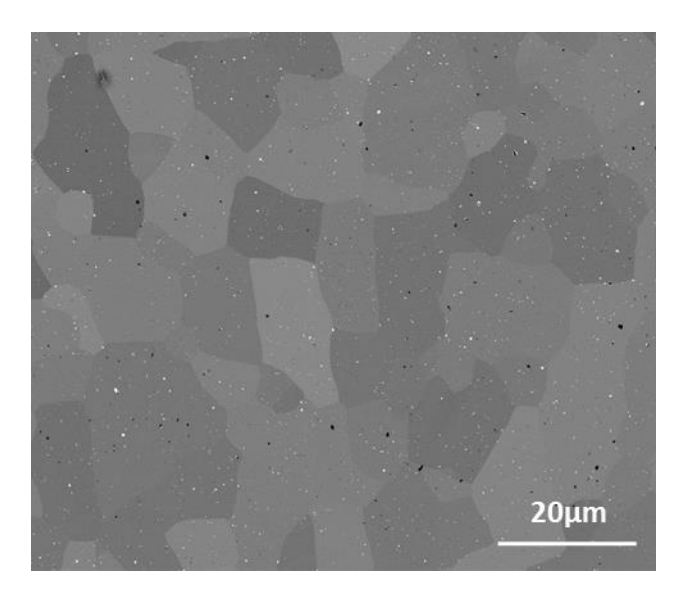
	С	Si	Mn	Мо	Cr	Al	Fe
Nominal composition				3.0	21.0	5.0	balance
Min					20.5		
Max	0.08	0.7	0.4		23.5		

Table 1. Chemical composition in mass% of Kanthal APMT according to the manufacturer Sandvik Materials Tecknology.



Figur 1. Bakåtspridd elektron SEM bild på ett polerat, något etsat APMT material

Figure 1. Backscattered electron SEM image of a polished, slightly etched APMT material



Figur 2. Bakåtspridd elektron SEM bild på ett polerat, något etsat APMT material som har varit exponerad I 1100°C i 24 timmar.

Figure 2. Backscattered electron SEM image of a polished, slightly etched APMT material that has been exposed to 1100°C for 24h

3 Experimental conditions

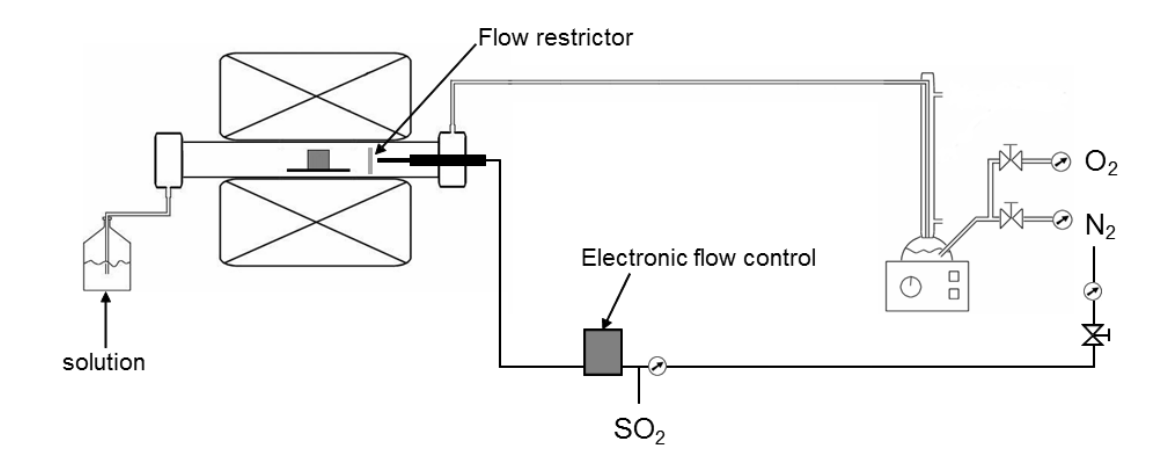
3.1 Material preparation

The material was supplied by Sandvik Heating Technology in the form of a 2-mm-thick sheet, from which square samples (1.5 x 1.5 cm) were cut. These samples were ground, and then polished with a 1- μ m diamond suspension in the final step. Before exposure, the samples were cleaned, sequentially with distilled water, acetone and ethanol, using ultrasonic agitation. The samples were then dried in an air flow, and their weights were recorded both before and after exposure.

A saturated solution of KCl in water/ethanol was used to apply KCl to the surfaces. The specimen was alternately sprayed and dried with warm air (\sim 35°C), so as to avoid the formation of large droplets on the surface. Each sample was treated with KCl at 0.1 mg per cm² of the material. The samples were then placed in a desiccator to cool, and the weight was recorded using a six-decimal-place Sartorious balance. The exposure was started immediately after the sample mass was recording.

3.2 Exposure equipment

Oxidation of the, Kanthal APMT, was conducted for 1, 24, 72 and 168 h at 600°C in 5 vol.% O_2 , 55 vol.% N_2 , 40 vol.% H_2O in a 300 ppm SO_2 atmosphere. The exposures were conducted in a horizontal tube furnace that was fitted with a silica tube (Figure 3). Three samples were placed on an alumina holder positioned parallel to the direction of the gas. 40% water vapor was added to the atmosphere by passing the gas through the humidifier and cooling it to the desired dew-point. The dry flow rate was calibrated using the Bios DC2 Flow Calibrator. The net gas flow velocity was 3.2 cm/s (1000 ml/min). All the components of the system were maintained at a temperature >100°C to prevent condensation of H₂O and formation of H₂SO₄. In addition, the samples were placed in the furnace 2 min before the water vapor was added to the exposure gas, so as to prevent condensation on the cool samples. SO₂ was added through a separate tube, and mixed with the rest of the gas inside the furnace about 20 cm upstream of the samples, at a temperature of about 300°C. This step was taken as a precaution for the exposures. The flow of SO_2 was controlled by a digital mass flow regulator. After passing the furnace tube, the gas was bubbled through a flask that contained a H₂O₂ solution. After exposure, the samples were allowed to cool in dry air. The samples were stored in a desiccator before the analyses of the oxide scales.



Figur 3. Exponeringsuppställning

Figure 3. Exposure set-up

3.3 Qualitative corrosion analysis of exposed material

The exposed APMT material was investigated by visual inspection and photographs of the surface. The samples were also investigated by a range of analytical techniques, such as gravimetric, SEM/EDX, XRD, AES, etc. All analysis was performed by HTC.

3.3.1 Gravimetric analysis

To get a rough estimation of the corrosion attack the weight of the samples were recorded on a six-decimal Sartorious balance before and after exposure.

3.3.2 X-ray diffraction (XRD)

The crystalline phase of the oxide grown on Kanthal APMT was analyzed by Grazing Incidence X-Ray Diffraction (GI-XRD). A Siemens D5000 powder diffractometer with Cu-Ka radiation was used for this purpose. Measurements were performed at $10^{\circ} < 20 < 70^{\circ}$ (incidence angle, 0.5°, step size, 0.05°).

3.3.3 Scanning electron microscopy (SEM)

The morphology of the samples was investigated by scanning electron microscopy, SEM. The resolution and depth of focus in an SEM is much higher than in an optical microscope, revealing more details of the corrosion attack. In addition, the SEM can be equipped with an Energy Dispersive X-rays system enabling analysis of the elemental composition in small areas of the sample. The samples were examined using the FEI Quanta 200 FEG ESEM and the Zeiss ULTRA 55 FEG SEM. The SEM had a field emission electron gun (FEG) and was equipped with an Oxford INCA energy dispersive X-ray (EDX)

system. For imaging and EDX analysis, an accelerating voltage of 3-20 kV was used.

3.3.4 Broad ion beam (BIB)

Cross sections through the oxide scale and the substrate were made using a Broad Ion Beam (BIB) instrument, GATAN Ilion+ TM. Prior to ion beam milling a mm thin Si or SiO_2 disc was attached to the oxide surface using TEM glue (M-Bond 610), thereafter a smaller piece of the sample was cut out and mounted on to a metal plate using silver glue. The samples were then place in the BIB instrument and two alternating Ar ion beams were milling a surface through the metal plate, the oxide scale and into the FeCrAl substrate. The resulting V-shaped cross sections were approximately 1 mm wide.

3.3.5 Auger electron spectroscopy (AES)

The AES analyses were performed with the PHI 660 Scanning Auger Microprobe using an accelerating voltage of 10 kV and a beam current of 100 nA. AES depth profiling was performed using ion sputtering with 3.5 keV Ar+. The analyzed area was 0.2-0.4 μm^2 . Semi-quantitative analyses were performed using the peak-to-peak height of the Auger transitions of a specific element together with sensitivity factors provided by PHI. The PHI-Matlab software and the linear least squares (LLS) routines were used to distinguish the oxide and metal components in the depth profiles. A sensitivity factor for oxygen was used for the AES profiles, resulting in 60% O for alumina. An additional sensitivity factor was needed for the O content to be correct for iron- and chromium oxide, which explains the high percentage of oxygen at the beginning of the AES profiles. Comparisons of TEM cross-sections and AES depth profiles have shown that the sputter rate of alumina is half that obtained using the calibration standard Ta₂O₅ 2,3 .

3.3.6 Ion chromatography (IC)

To determine the levels of water-soluble anions (Cl $^-$, SO $_4$ ^{2 $^-$}, and CrO $_4$ ^{2 $^-$}) on the exposed samples, the Dinoex ICS-90 system was used. The anions were analyzed with an IonPac AS4A-SC analytic column and 1.8 mM NaHCO $_3$ /1.7 mM NaHCO $_3$ was used as the eluent. The flow rate was 2 ml/min. This system was also used to control the amount of SO $_2$ in the exposure gas by analyzing the H $_2$ O $_2$ solution.

3.3.7 Secondary ion mass spectrometry (SIMS)

TOF-SIMS analysis was performed using the TOF-SIMS V instrument (ION-TOF GmbH, Münster, Germany) that was equipped with a 25-keV Bismuth LMIG analysis gun and a 10-keV Cs sputter gun, at the National Center for Imaging Mass Spectrometry, Chalmers University of Technology, Gothenburg, Sweden.

Depth profiling and imaging were performed in the non-interlaced mode with 1 frame of analysis, 1 s of sputtering, and 0.5 s pausing per cycle, while the floodgun was using for charge compensation. The Bi-LMIG was set in the high

current bunched mode (mass resolution m/ Δ m, 6000; focus of the ion beam, 1 µm) using Bi1 ions with a target current of 0.2 pA, while Cs ions at 3 keV and 0.22 nA were used for sputtering. The analysis field of view was set to 25 x 25 µm, and the sputter area was set to 100 x 100 µm. The dose density of Cs was 2.03e+17 (1/cm 2) and the total dose density of Bi was 1.25e+14 (1/cm 2).

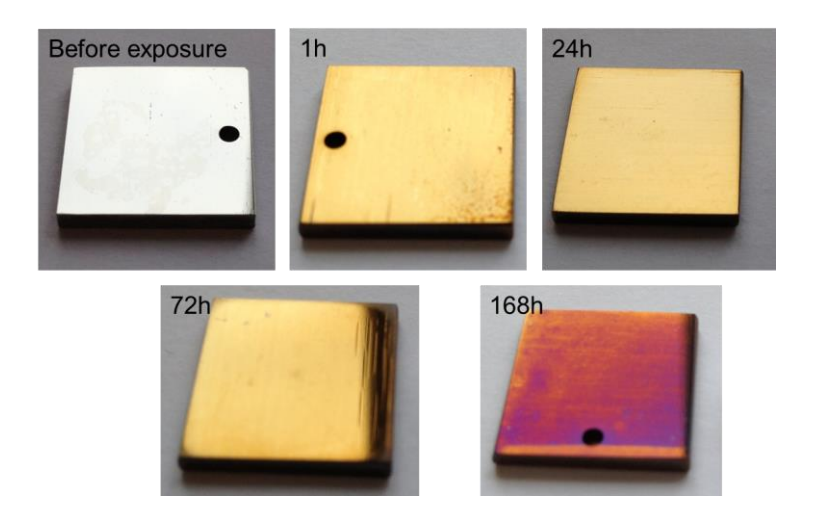
All the image and depth profile analyses were performed using the ION-TOF Surface Lab software (ver. 6.3 (ION-TOF)).

4 Results

4.1 The effect of SO₂ in the presence of H₂O

4.1.1 Macro appearance

Before exposure the polished FeCrAl alloy, Kanthal® APMT, exhibited a grayish metallic luster (Figure 4). After exposure for 1-168 h to 5 % O_2 + 40 % H_2O + 300 ppm SO_2 at 600°C, the surface had a yellowish luster (Figure 4), likely due to the formation of an oxide scale with a thickness corresponding to the interference color. After exposure for 168 h, the material surface exhibited a mixture of yellow and purple colors.



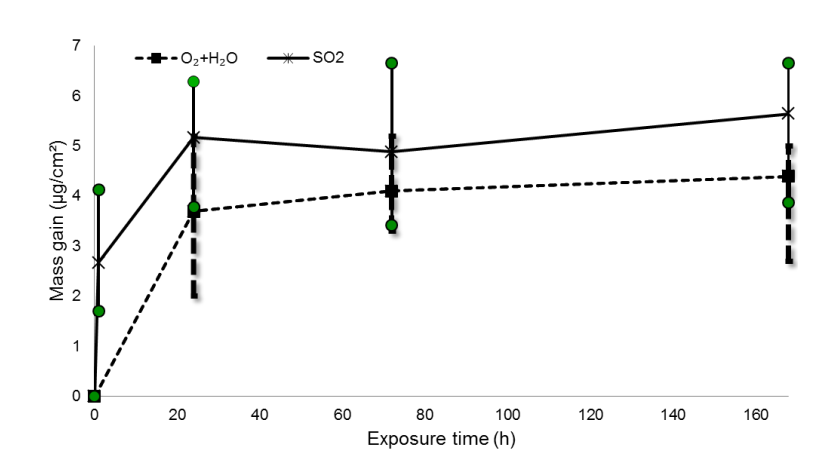
Figur 4. Bilder på Kanthal APMT före och efter exponering i 600° C 5 % O_2 + 40 % H_2O + 300 ppm SO_2 .

Figure 4. Images of Kanthal APMT before and after exposure at 600°C in 5 % O_2 + 40 % H_2O + 300 ppm SO_2 .

4.1.2 Mass gain

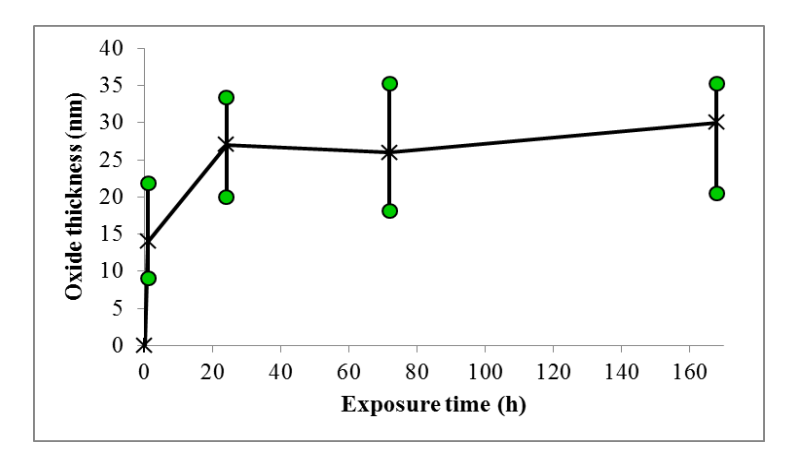
Figure 5 shows the mass gain versus exposure time for Kanthal APMT in an environment of 5 % O_2 + 40 % H_2O + 300 ppm SO_2 . The mass gain of the samples is very low, with the largest mass gain being <7 μ g/cm². The main mass gain takes place at the start (<24 h) and thereafter increases approximately linearly with time. The oxide thicknesses were calculated from the mass gain values (Figure 6). It was presumed that the oxide scale consisted of pure and dense alumina. It is useful to compare the oxide thicknesses with the results obtained using the other analytic tools presented below. In Figure 5, the mass gain of Kanthal APMT exposed to 5 % O_2 + 40

% H₂O + 300 ppm SO₂ is compared with the mass gain obtained in the same atmosphere but in the absence of SO₂. Although the average values are lower in the absence of SO₂, the error bars for the two exposure atmospheres overlap. Thus, there is no significant difference in the mass gains of APMT between the two exposure environments.



Figur 5. Massökning mot exponeringstid för Kanthal APMT vid 600° C i 5% $O_2 + 40\%$ H_2 O och 5% $O_2 + 40\%$ H_2 O + 300 ppm SO_2 .

Figure 5. Mass gain versus exposure time for Kanthal APMT at 600° C in 5 % O_2 + 40 % H_2 O and 5 % O_2 + 40 % H_2 O + 300 ppm SO_2 .

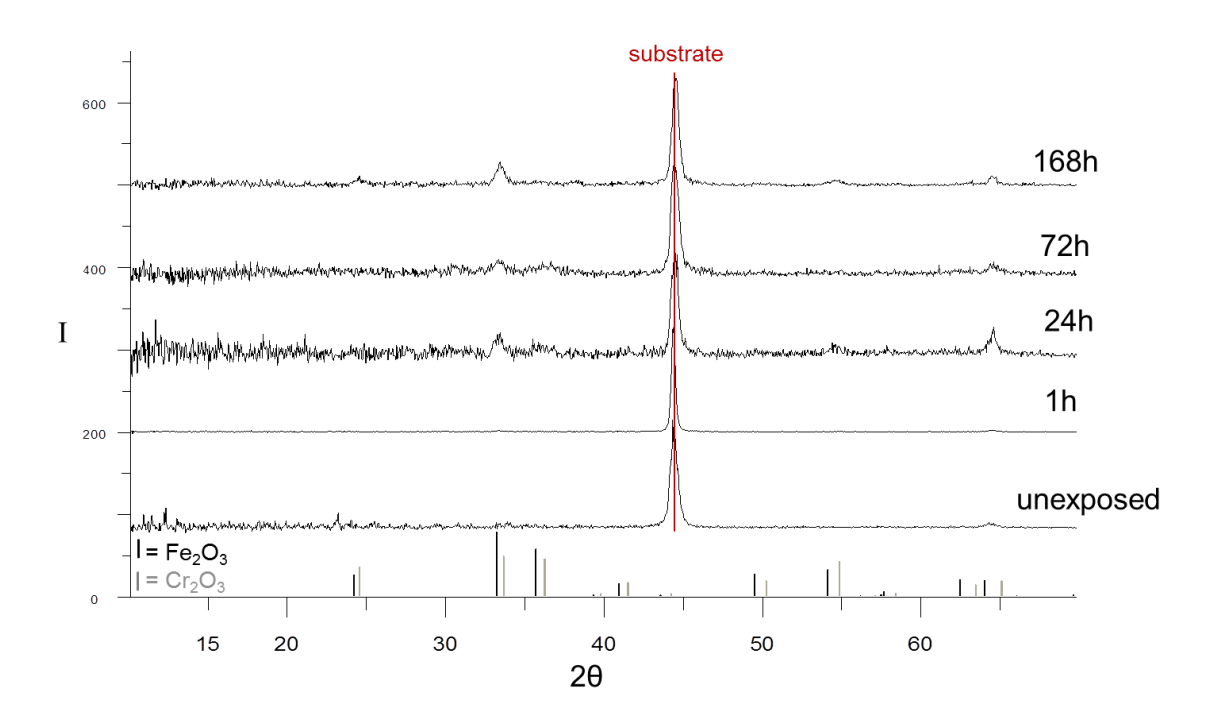


Figur 6. Beräknad oxidtjocklek mot exponeringstid för Kanthal APMT vid 600°C i 5 % O_2 + 40 % H_2O + 300 ppm SO_2 .

Figure 6. Calculated oxide thickness versus exposure time for Kanthal APMT at 600°C in 5 % O₂ + 40 % H₂O + 300 ppm SO₂.

4.1.3 Crystalline oxide products

After exposure of Kanthal[®] APMT to 5 % O_2 + 40 % H_2O + 300 ppm SO_2 , the crystalline oxide product $(Fe,Cr)_2O_3$ was detected by XRD on the surface of the alloy for all the exposure periods tested (Figure 7). The XRD diffractogram is similar for samples exposed without SO_2 (not shown). Hence the same oxide product is formed with and without SO_2 in the exposure gas.

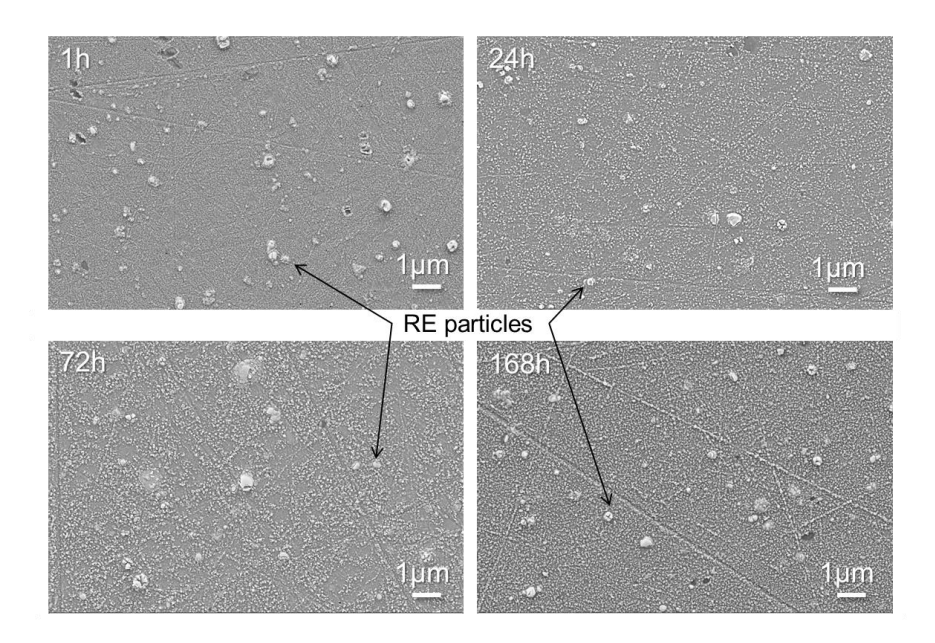


Figur 7. XRD diffraktogram av materialet APMT före och efter exponering mellan 1-168h i 5 $\% O_2 + 40 \% H_2O + 300 ppm SO_2$.

Figure 7. XRD diffractogram of the alloy APMT before and after exposure for 1-168h in 5 % $O_2 + 40 \% H_2O + 300 \text{ ppm } SO_2$.

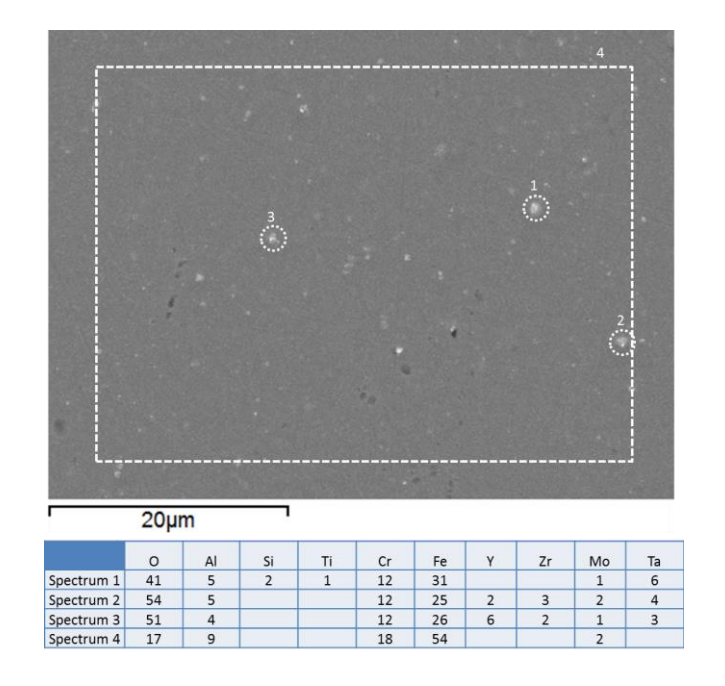
4.1.4 SEM/EDX

Figure 8 shows the secondary electron SEM images of the surface of the alloy after exposure for 1–168 h. The surface appears flat without any large oxide protrusions. According to the EDX analysis (Figure 9), the bright particles, which have a diameter of approximately 300 nm are reactive element particles. Some smaller nanometer-sized bright particles are also evident, scattered across the entire surface. EDX analysis of an area (3 x 3 μ m) revealed the same elemental composition as the unexposed alloy, showing that the oxide product formed is very thin, which is in accordance with the mass gain results.



Figur 8. Sekundär elektron SEM bilder av materialets yta efter 1-168 timmars exponering i 5 $\% O_2 + 40 \% H_2O + 300 \text{ ppm } SO_2$.

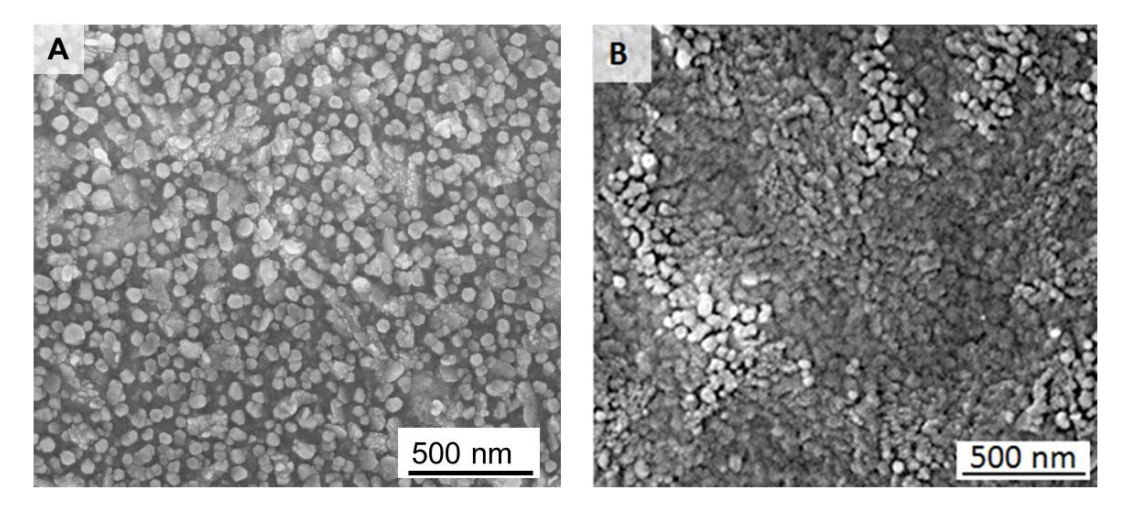
Figure 8. Secondary electron SEM images of the surfaces of the alloy exposed for 1-168h in $5 \% O_2 + 40 \% H_2O + 300 \text{ ppm } SO_2$.



Figur 9. Sekundär elektron SEM bilder samt EDX analyser av materialets yta efter 72 timmars exponering i 5 % O_2 + 40 % H_2O + 300 ppm SO_2 .

Figure 9. Secondary electron SEM images and EDX analyses of the surfaces of the alloy exposed for 1-168h in 5 % O_2 + 40 % H_2O + 300 ppm SO_2 .

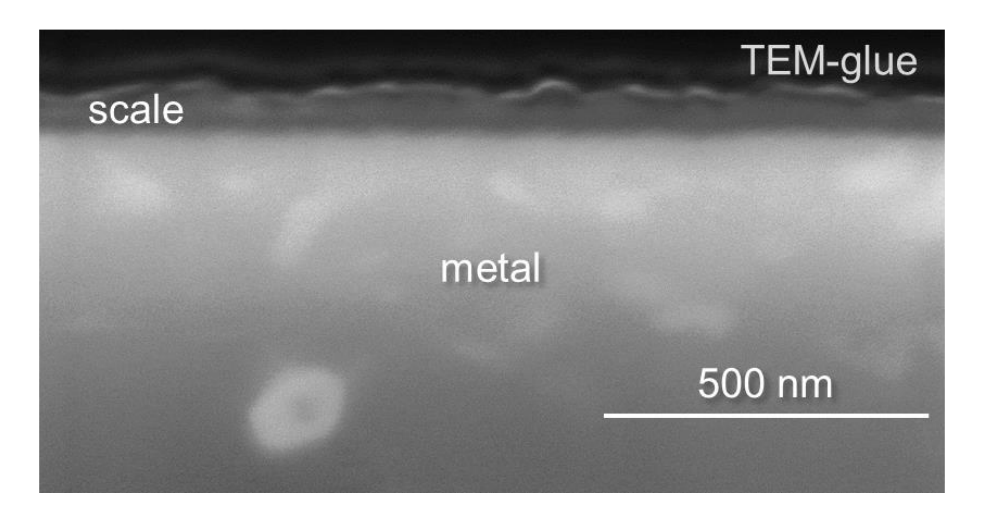
Figure 10 show a secondary electron SEM image of the surface of the alloy APMT exposed for 168 h with SO_2 (A) and an in-lens SEM image without (B) SO_2 . Both images reveal a relatively flat surface without any large oxide protrusions.



Figur 10. (A) Sekunär elektron SEM bild av APMT materialets yta efter 168 timmars exponering i 5 % O_2 + 40 % H_2O + 300 ppm SO_2 , (B) In-lens SEM bild av APMT materialets yta efter 168 h exponering i 5 % O_2 + 40 % H_2O .

Figure 10. (A) Secondary electron SEM image of the surface of the alloy APMT exposed for 168h in 5 % O_2 + 40 % H_2O + 300 ppm SO_2 , (B) In-lens SEM image of the surface of alloy APMT after exposure in 5 % O_2 + 40 % H_2O .

Figure 11 shows a cross-section of the scale formed on the APMT after 168 h of exposure in the presence of SO_2 . A thin continuous scale is formed on the material surface. The scale has a thickness of approximately 60 nm, which is somewhat higher than the calculated value (~ 30 nm). However, the exact thickness of the oxide is difficult to determine, and the calculated value is for a dense alumina.

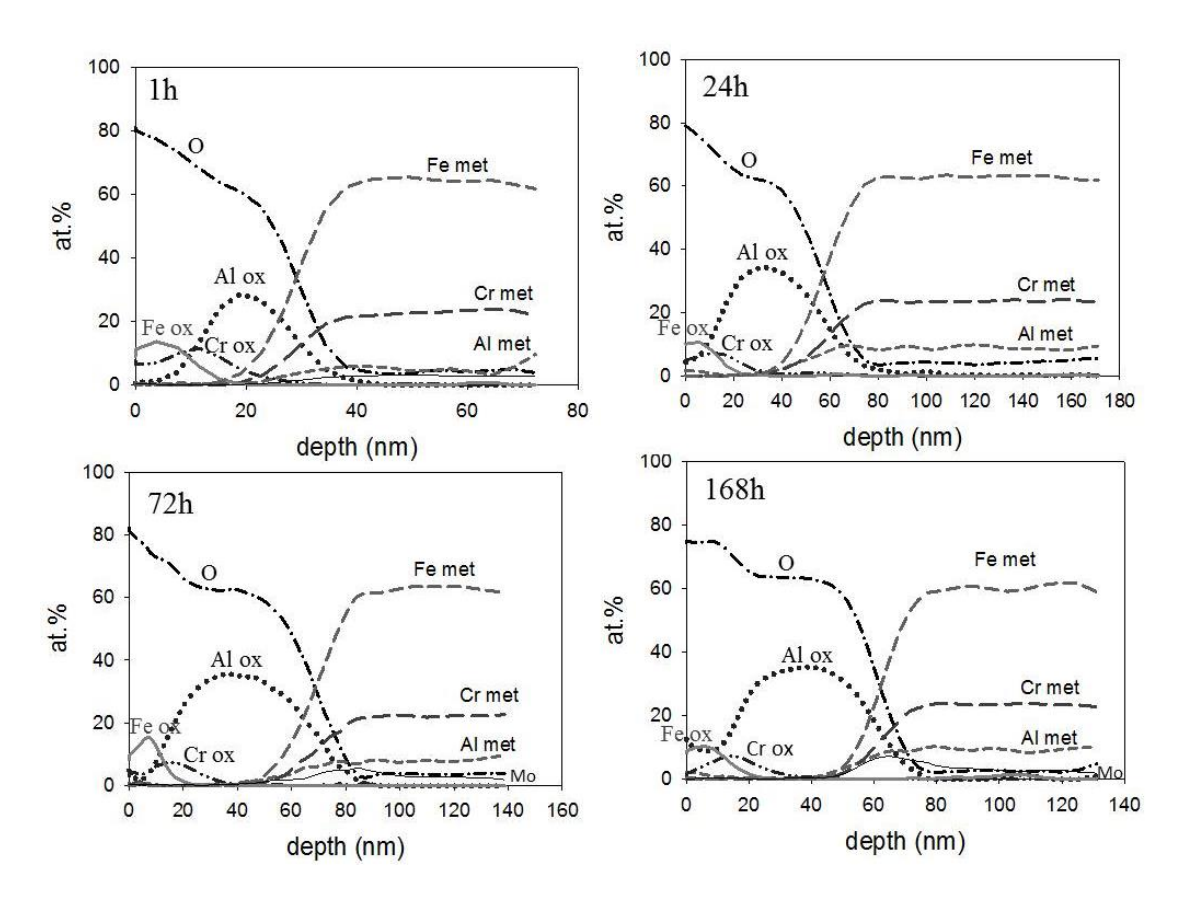


Figur 11. Sekundär elektron SEM bild av ett tvärsnitt av APMT efter 168 timmars exponering i 5 % O_2 + 40 % H_2O + 300 ppm SO_2 .

Figure 11. Secondary electron SEM image of the cross section of APMT after exposure for 168h in 5 % O_2 + 40 % H_2O + 300 ppm SO_2 .

4.1.5 Elemental depth profiles

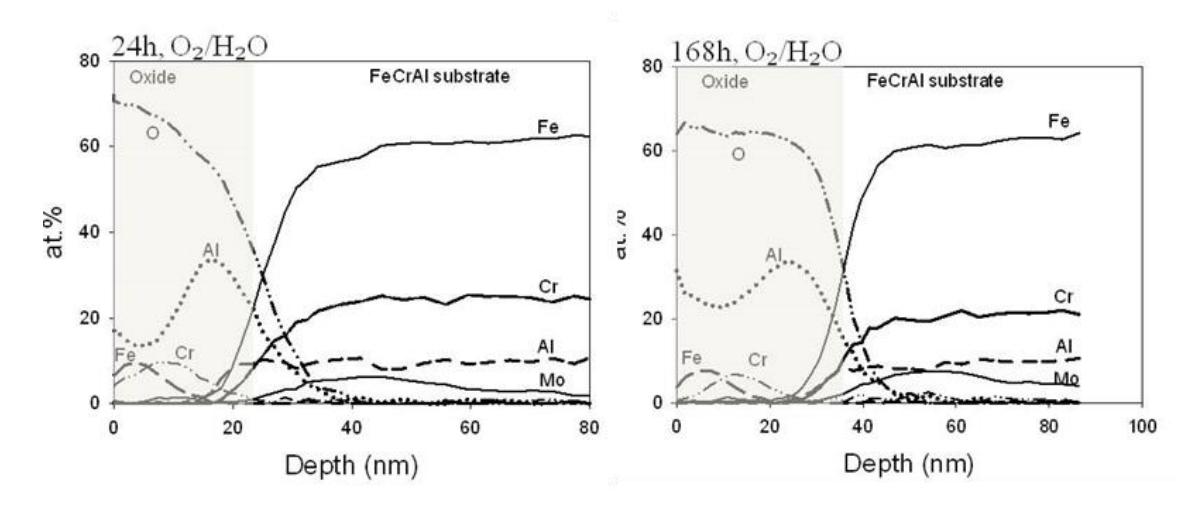
Figure 12 show AES depth profiles of the alloy APMT exposed for $1-168\,h$ in the presence of SO_2 . After 1 h exposure, the profiles show an outer Fe-rich oxide, followed by a Cr-rich oxide, and with an aluminum-rich oxide closest to the metal substrate. With longer exposure times, the alumina is thicker and the outer oxide is enriched in Al. The Cr and Fe containing oxide is detected by XRD, showing $(Fe,Cr)_2O_3$, but no alumina was detected by XRD indicating a poorly diffracting oxide, i.e. amorphous oxide. AES analysis of the surface shows the existence of S for all exposure times. In addition, S was detected between the Cr-rich oxide and the Al-rich oxide at all exposure times. However, the concentration of S was very low, which means that it would not be visible in the AES plots. The oxide thickness increased with exposure time, and the observed values are closed to the calculated values.



Figur 12. AES djup profiler från legeringen APMT exponerad i 1 – 168 timmar i 5 % O_2 + 40 % H_2O + 300 ppm SO_2 .

Figure 12. AES depth profiles of alloy APMT exposed for 1 - 168 h in 5 % O_2 + 40 % H_2O + 300 ppm SO_2 .

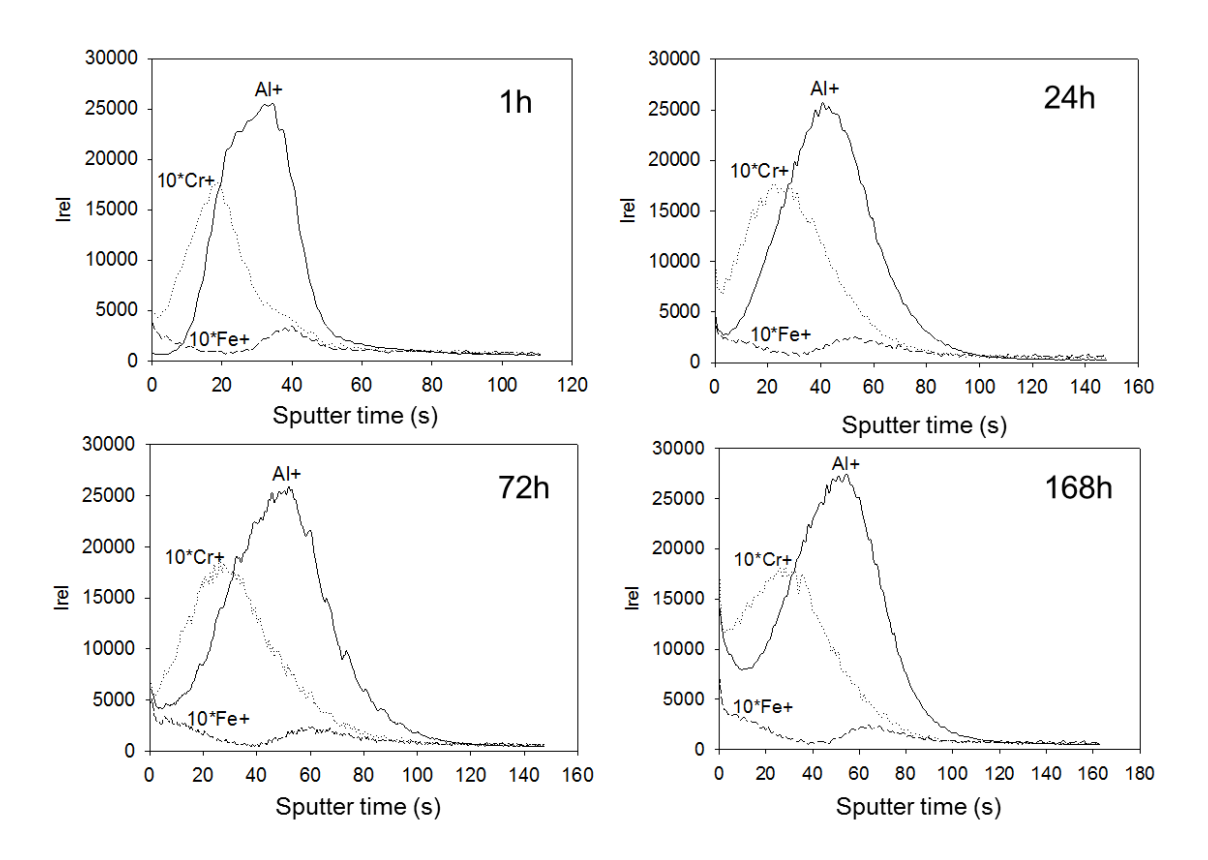
Figure 13 shows the AES depth profiles of APMT after 24 h and 168 h of exposure in the absence of SO_2 ⁴. The oxide appears to be built up in the same way as during exposure to SO_2 , with the exception that an Al-rich outer layer is added. These results indicate that sulfur inhibits outward growth of alumina.



Figur 13. AES djup profiler från legeringen APMT exponerad i 24 och 168 timmar i 5 % O_2 + 40 % H_2O .

Figure 13. AES depth profiles of alloy APMT exposed for 24 and 168 h in 5 % O_2 + 40 % H_2O .

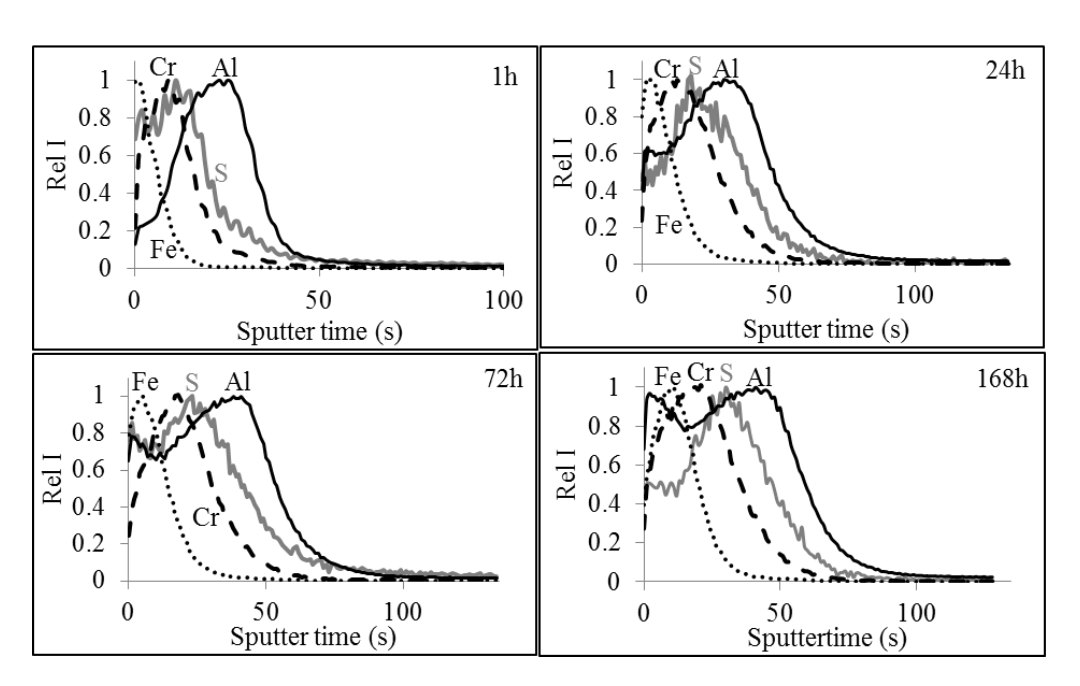
The SIMS depth profiles of positive ions in Figure 14 are in accordance with the AES depth profiles; After 1 hour exposure the profiles show an outer Fe rich oxide followed by a Cr rich oxide and thereafter an aluminium rich oxide closest to the metal substrate. After longer exposure times the alumina oxide grows in thickness and the outer oxide also gets enriched in Al.



Figur 14 SIMS djupprofil av positiva joner av legeringen APMT efter exponering i 1 – 168 timmar i närvaro av SO₂.

Figure 14. SIMS depth profiles of positive ions of alloy APMT exposed for 1 – 168 h in the presence of SO₂.

The SIMS depth profiles of the negative ions of APMT exposed in the presence of SO_2 , as shown in Figure 15, are in agreement with the the SIMS depth profiles of the positive ions and the AES depth profiles, in that they show a layered oxide in the order Fe, Cr, Al, and metal, as well as enrichment of Al in the outer part with time. In addition, enrichment of sulfur was detected between the Cr-rich oxide and the Al-rich oxide for all the exposure times. However, sulfur was not detected at the oxide/metal interface.

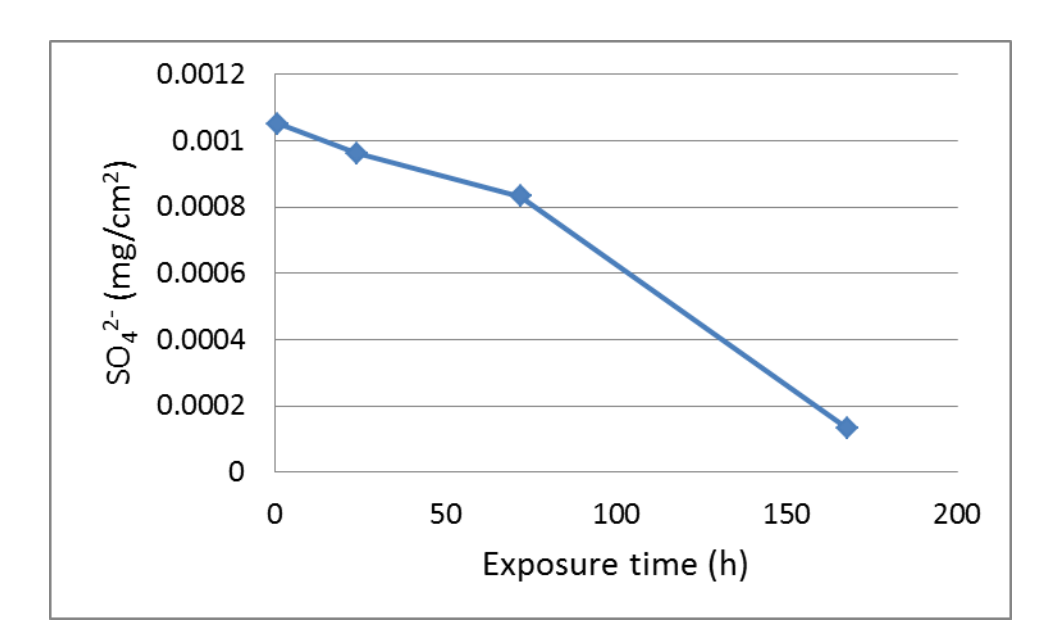


Figur 15. SIMS djupprofil av negativa joner av legeringen APMT efter exponering i 1 – 168 timmar i närvaro av SO₂.

Figure 15. SIMS depth profiles of negative ions of alloy APMT exposed for 1 – 168 h in the presence of SO₂.

4.1.6 Water-soluble oxide products

Figure 16 shows the levels of $SO_4^{2^-}$ detected by IC analysis after extraction of the soluble surface products formed on the APMT during exposure in the presence of SO_2 . The levels of detected $SO_4^{2^-}$ were very low for all exposure times, being highest after 1 h of exposure at $\sim\!0.001$ mg/cm², and declining to $<\!0.0002$ mg/cm² after 168 h of exposure. These outcomes are in accordance with the AES results, whereby low levels of S were found on the surface.



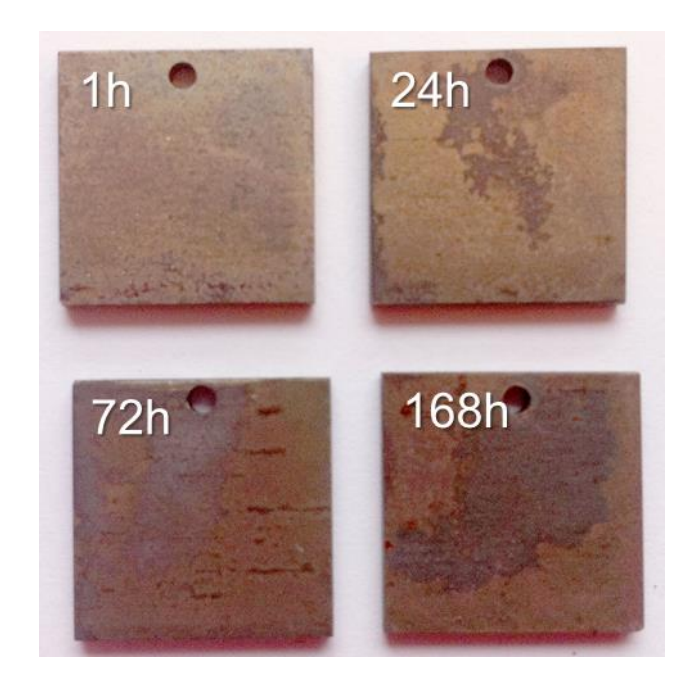
Figur 16 IC analys av de lösliga oxidprodukterna som bilda på Kanthal APMT efter 1 – 168 timmars exponering i 5 % O_2 + 40 % H_2O + 300 ppm SO_2 .

Figure 16. IC analysis of soluble oxide products formed on alloy APMT after exposure for 1 – $168 \text{ h in } 5 \% \text{ O}_2 + 40 \% \text{ H}_2\text{O} + 300 \text{ ppm SO}_2$.

4.2 The effect of SO₂ in the presence of KCl

4.2.1 Macro apperance

After exposure of Kanthal APMT for 1-168 hours to $5\%~O_2$, $40\%~H_2O$, $300~ppm~SO_2$, and KCl, the surfaces of the alloy showed uneven corrosion. (Figure 17).

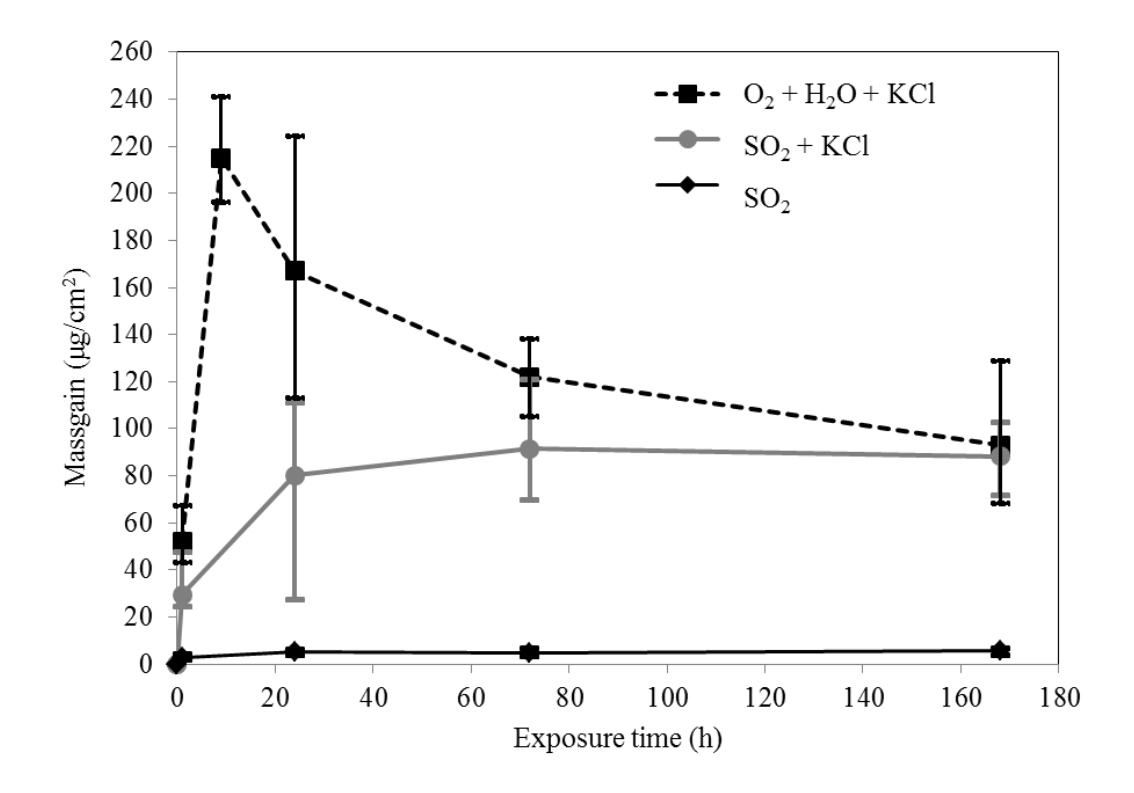


Figur 17. Bilder på Kanthal APMT efter exponering i 600° C 5 % O_2 + 40 % H_2 O + 300 ppm SO_2 + KCI

Figure 17. Images of Kanthal APMT after exposure at 600° C in 5 % O_2 + 40 % H_2 O + 300 ppm SO_2 + KCl.

4.2.2 Mass gains

Figure 18 shows the mass gain versus exposure time for APMT in the presence of a combination of SO_2 and KCl. The mass gain curve obtained for the environments $5\%~O_2$, $40\%~H_2O$ and $300~ppm~SO_2$ and $5\%~O_2$, $40\%~H_2O$, and KCl 4 is included for the purpose of comparison. The mass gain in this case was about 20-fold higher than the mass gain observed in the absence of KCl. The increase in mass was initially rapid but it declined thereafter, reaching a plateau after 24 h of exposure. The relatively large scatter at the beginning of the exposure in the presence of KCl indicates the startup of a reaction.

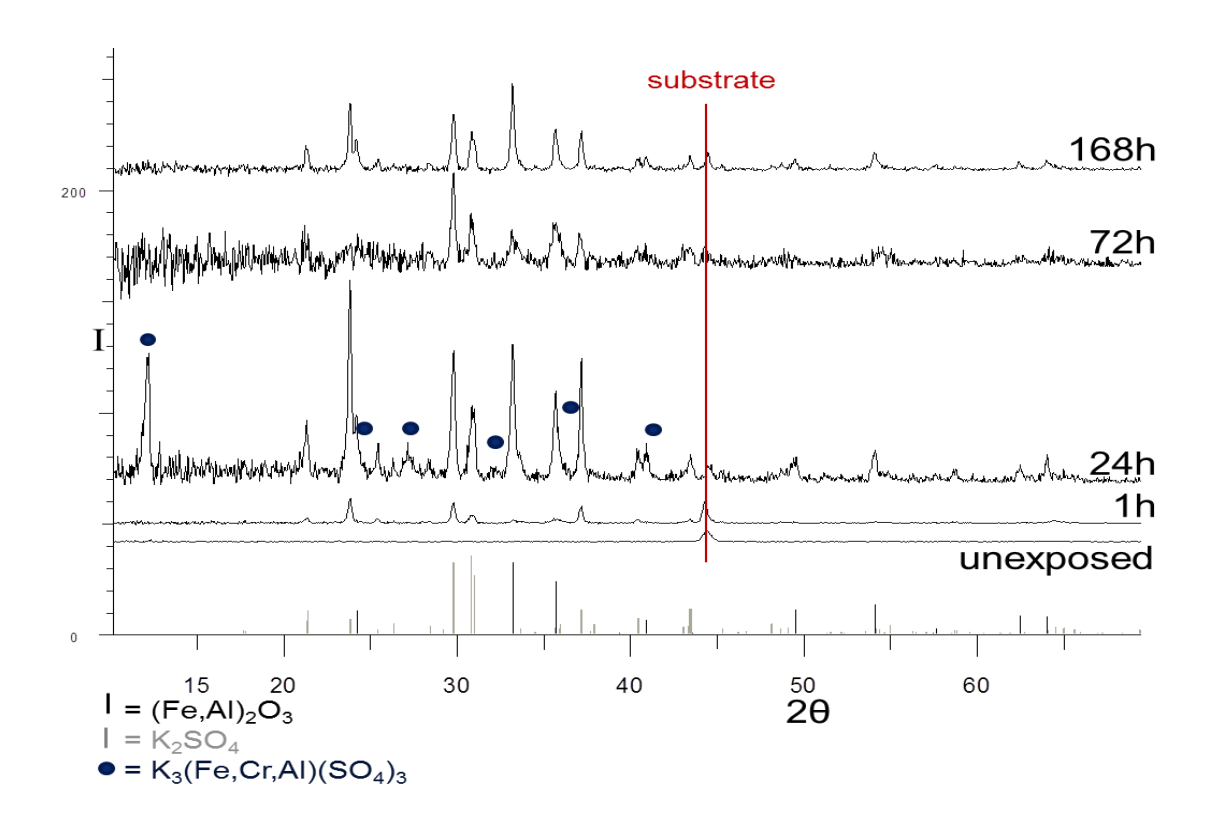


Figur 18. Massökning mot exponeringstid för Kanthal[®] APMT vid 600°C i 5 % O_2 + 40 % H_2O + 300 ppm SO_2 och 5 % O_2 + 40 % H_2O + 300 ppm SO_2 + KCl.

Figure 18. Mass gain versus exposure time for Kanthal[®] APMT at 600°C in 5 % O_2 + 40 % H_2O + 300 ppm SO_2 and 5 % O_2 + 40 % H_2O + 300 ppm SO_2 + KCl.

4.2.3 Crystalline oxide products

The X-ray diffraction analysis (Fig. 19) showed that the main crystalline oxide products present at all exposure times were $(AI,Cr,Fe)_2O_3$ and K_2SO_4 . In addition, $K_3(AI,Fe,Cr)(SO_4)_3$ was present after 24 h of exposure. The diffraction peaks for KCl overlapped with the other peaks, making it impossible to determine whether any KCl was present. Peaks corresponding to chromates were not detected.

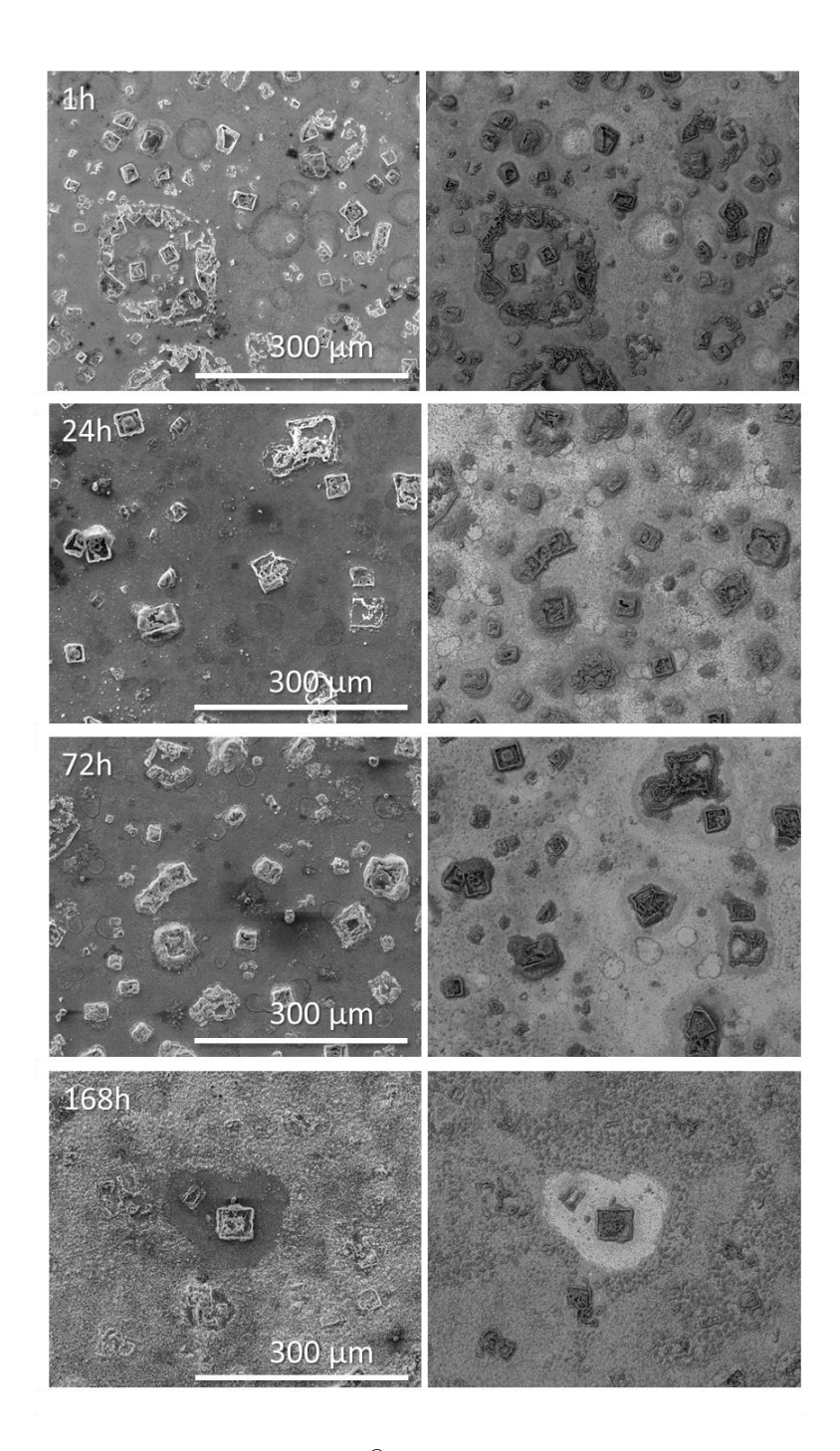


Figur 19. Röntgen diffraktogram från Kanthal APMT efter exponering vid 600° C i 5% O₂ + 40% H₂O + 300 ppm SO₂ + KCl.

Figure 19. XRD diffractogram from Kanthal APMT after exposure at 600°C in 5 % O_2 + 40 % H_2O + 300 ppm SO_2 + KCl.

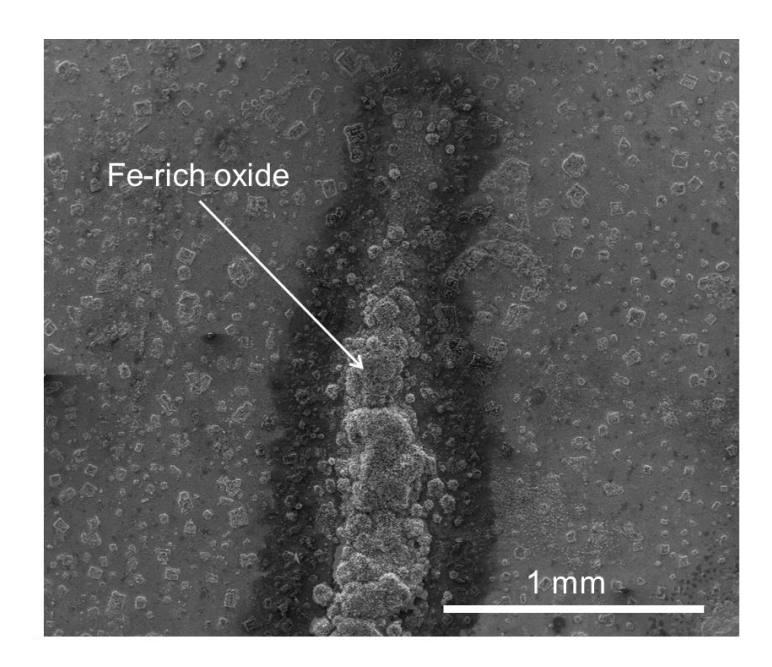
4.2.4 SEM/EDX

Figure 20 shows the backscattered SEM surface images of APMT exposed to the environment of 5% O_2 , 40% H_2O , 300 ppm SO_2 , and KCl. While the images were taken from representative regions of the surface, some regions of the sample exposed for 1 h resembled regions of the samples exposed for 168 h. Furthermore, in the samples exposed for 24-168 h, there were a few regions with high levels of corrosion (Fig 21).



Figur 20. SEM bilder av ytan på Kanthal[®] APMT efter exponering i 1-168 timmar vid 600°C i 5 % O_2 + 40 % H_2O + 300 ppm + KCl. Sekundära bilder till vänster och bakåtspridda till höger.

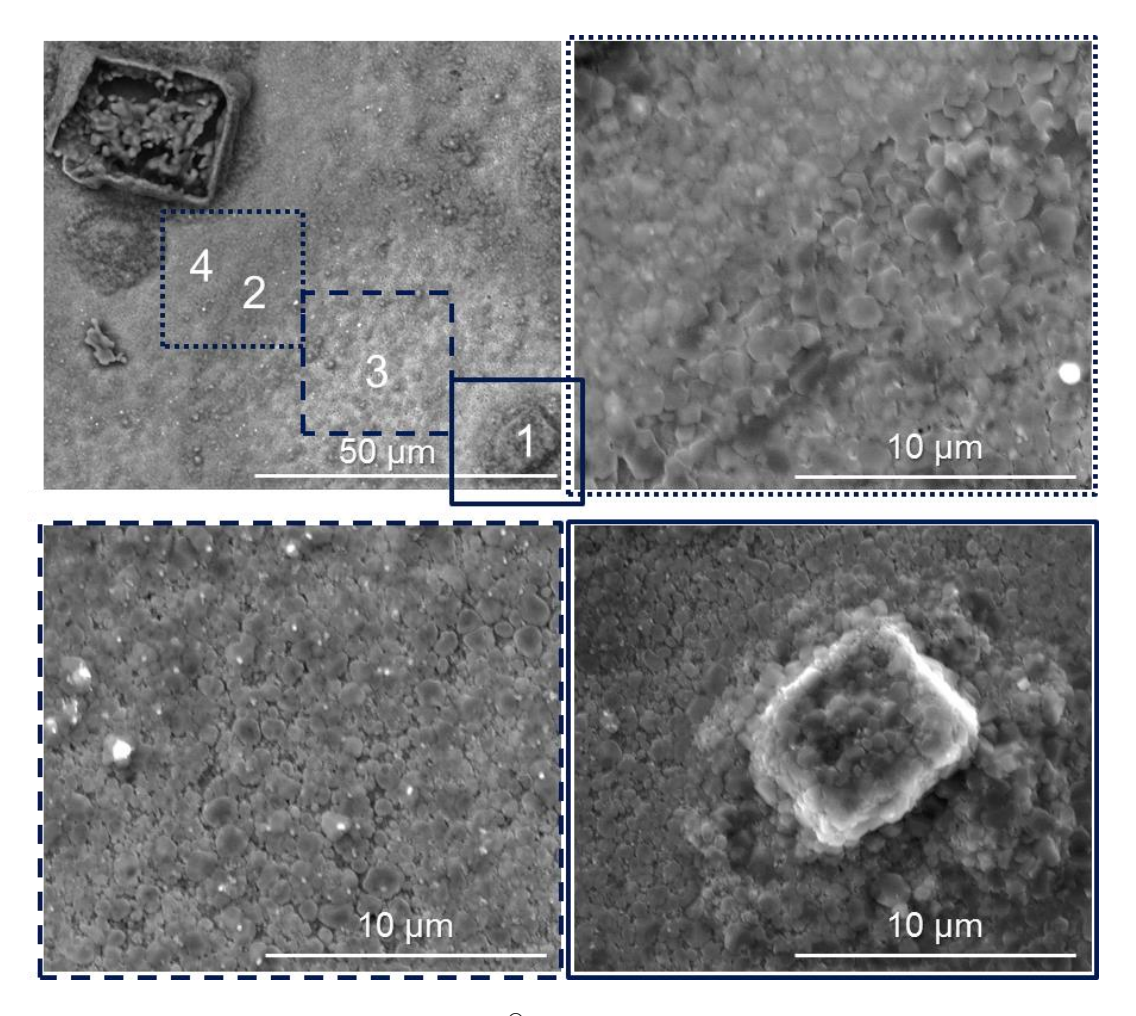
Figure 20. SEM surface images of Kanthal[®] APMT after exposure for 1-168h at 600°C in 5 % O_2 + 40 % H_2O + 300 ppm SO_2 + KCl. Secondary images to the left and backscattered to the right.



Figur 21. Sekundär SEM bild på ytan av Kanthal[®] APMT efter exponering i 72 timmar vid 600°C i 5 % O₂ + 40 % H₂O + 300 ppm + KCl.

Figure 21. Secondary SEM image of the surface of Kanthal[®] APMT after exposure for 72 h at 600° C in 5 % O_2 + 40 % H_2 O + 300 ppm SO_2 + KCl.

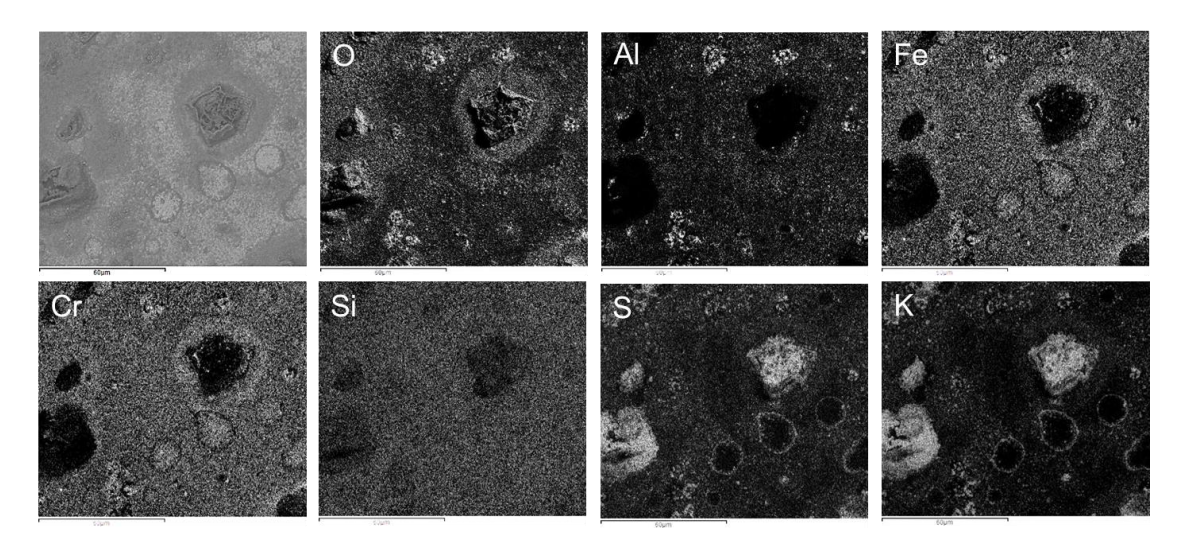
Figure 22 shows images of the surface of APMT after 1 h of exposure to the environment of 5% O2, 40% H2O, 300 ppm SO2, and KCl. The lowmagnification image (50 μ m bar) was taken in the backscattered mode, whereas the remaining three high-magnification images were captured in the secondary mode. In the backscattered image, the four following regions are labeled with numbers and enlarged in the secondary images: 1) regions that have the shape of the former KCl particles; 2) regions with dark rings (backscattered mode); 3) regions with bright base oxide; and 4) regions with dark base oxide. Judging from the secondary images, it seems that the entire surface (encompassing all the regions) is covered by rounded (about 1 µm in diameter) particles. EDX analysis of the different regions showed that the surface was rich in S, K, and O, so it is reasonable to conclude that these particles are K₂SO₄, as detected by XRD. The regions that have the shape of the former KCl particles are likely to represent KCl that has reacted with the SO₂ in the gas, thereby forming K₂SO₄ with maintenance of the shape of the KCl particle. The ring-shaped regions are likely due to remains from a vaporized droplet from the application of KCl, which would give the KCl particles the appearance of a ring structure. After the application of KCI, small residues of KCl remain between the discrete KCl particles 5, which explains the formation of K₂SO₄ from the larger KCl particles and the formation of rings. The EDX analyses revealed the presence of chlorine (CI) in the base oxide and dark regions, the atom% being 0:45%, Al:4%, S:6% Cl:2%, K:10% Cr:10%, Fe:23% and O:50%, Al:3%, S:8% Cl:2%, K:13% Cr:8%, Fe:16%, respectively. The observed chlorine may originate from unreacted KCI particles (albeit not detected by XRD) or they may be the result of alloy chlorination.



Figur 22. SEM bilder på ytan av Kanthal[®] APMT efter exponering i 1 timma vid 600°C i 5 % O_2 + 40 % H_2O + 300 ppm + KCl. Övre vänstr bilden är tagen med bakåtspridda elektroner, de övriga bilderna är tagna med sekundära elektroner.

Figure 22. SEM surface images of Kanthal[®] APMT after 1 h exposure at 600°C in 5 % O_2 + 40 % H_2O + 300 ppm SO_2 + KCl. The upper left image is taken I backscattered mode and the other images are taken in the secondary mode.

After 24 h of exposure, K and S were still detected almost everywhere on the surface of the alloy. The EDX map (Fig. 23) reveals regions that overlap with the maps for Al, Cr, Fe, K, S, and O, likely corresponding to $K_3(Fe,Cr,Al)(SO_4)_3$, as detected using XRD. Chlorine was only detected in those few regions where heavy oxidation had occurred (Fig. 24). The atom% Cl detected was in the range of 2-12%, with one point having an composition of O:68%, Al:0%, S:2% Cl:11%, K:3% Cr:11%, Fe:5%.



Figur 23. SEM EDX kartor på Kanthal[®] APMT efter 24 h exponering vid 600°C i 5 % O_2 + 40 % H_2O + 300 ppm + KCl.

Figure 23. SEM EDX maps of Kanthal® APMT after 24 h exposure at 600°C in 5 % O_2 + 40 % H_2O + 300 ppm SO_2 + KCl.

5.74

0.78

4.32

14.62

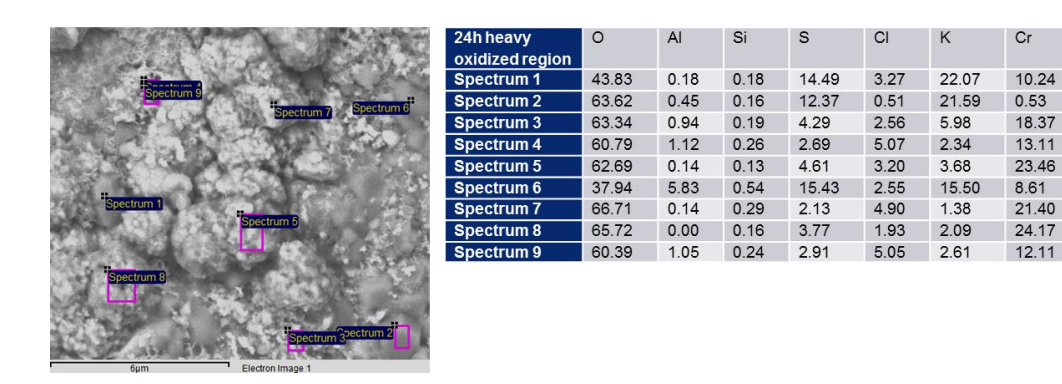
2.10

13.61

3.06

2.16

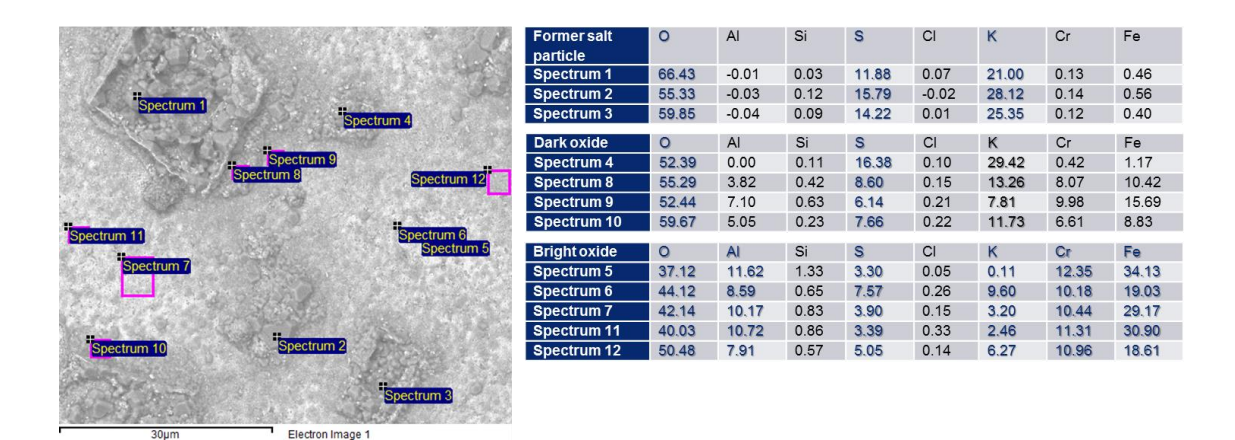
15.65



Figur 24. SEM bild och EDX analyser på Kanthal[®] APMT efter 24 timmars exponering vid 600°C i $5 \% \text{ O}_2 + 40 \% \text{ H}_2\text{O} + 300 \text{ ppm} + \text{KCI}$.

Figure 24. SEM image and EDX analyses of Kanthal[®] APMT after 24 h exposure at 600°C in $5\% O_2 + 40\% H_2O + 300$ ppm $SO_2 + KCI$.

Figure 25 shows a backscattered SEM image and EDX analyses from Kanthal $^{\otimes}$ APMT after exposure for 72 hours in O_2 + H_2O + SO_2 + KCl environment. After 72 hours oxidation K and S was still detected at all regions on the surface and Cl was detected at a few heavily oxidized regions, which accords with the results obtained for the material exposed for 24 hours (Figure 26). The Cl content is especial high at regions where the surface appears partly detached.



Figur 25. SEM bild och EDX analyser på Kanthal[®] APMT efter 72 timmars exponering vid 600°C i 5 % O_2 + 40 % $H_2\text{O}$ + 300 ppm + KCl.

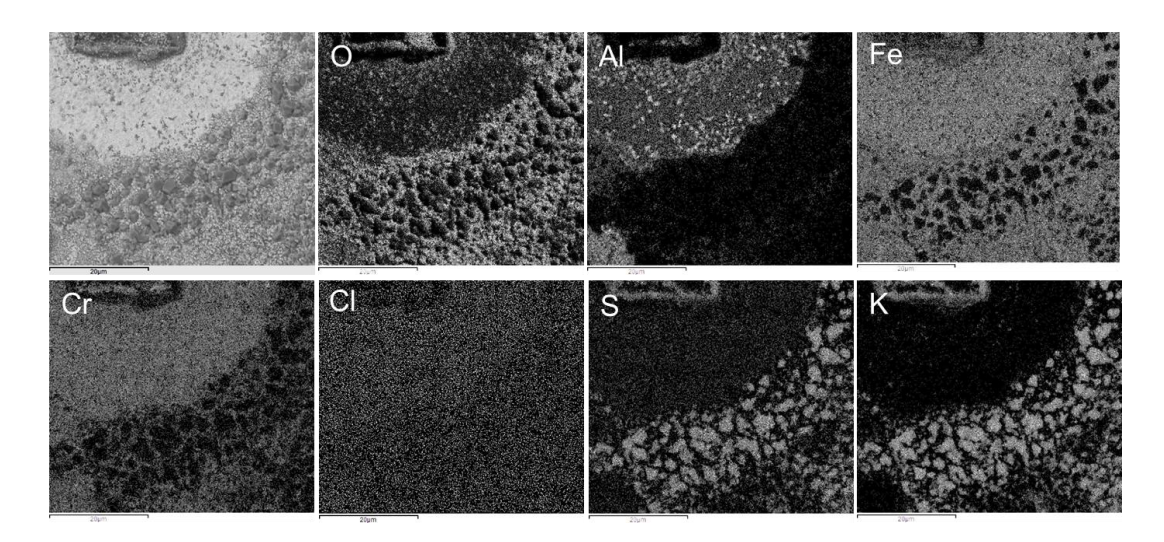
Figure 25. SEM image and EDX analyses of Kanthal[®] APMT after 72 h exposure at 600°C in $5\% O_2 + 40\% H_2O + 300$ ppm $SO_2 + KCI$.

Spectrum 10	Spectrum	0	Al	Si	S	CI	K	Cr	Fe
The second of the second control of the seco	Spectrum 1	63.18	0.01	0.08	1.25	-0.01	0.76	1.52	33.21
Spectrum 6	Spectrum 2	55.84	0.16	0.08	1.98	0.01	2.08	1.51	38.35
Spectrum 9 Spectrum 5	Spectrum 3	41.95	7.42	0.59	2.76	2.01	1.79	8.54	34.95
Spectrum 7	Spectrum 4	62.73	0.84	0.08	6.48	11.57	5.36	2.52	10.42
	Spectrum 5	68.23	4.60	0.18	3.22	10.62	3.15	4.85	5.15
Spectrum 3	Spectrum 6	57.18	-0.07	0.14	14.72	1.20	25.38	0.41	1.04
	Spectrum 7	71.44	0.47	0.00	1.16	2.55	1.09	5.73	17.56
Spectrum 4	Spectrum 8	64.23	4.49	0.11	1.79	8.48	1.69	11.42	7.80
	Spectrum 9	52.78	8.42	0.62	1.89	0.65	0.63	12.40	22.59
	Spectrum 10	65.46	1.65	0.19	10.82	0.31	18.51	1.14	1.92
Spectrum 6 Spectrum 2									
100µm Electron Image 1									

Figur 26. SEM bild och EDX analyser på Kanthal[®] APMT efter 72 timmars exponering vid 600°C i 5 % O₂ + 40 % H₂O + 300 ppm + KCl.

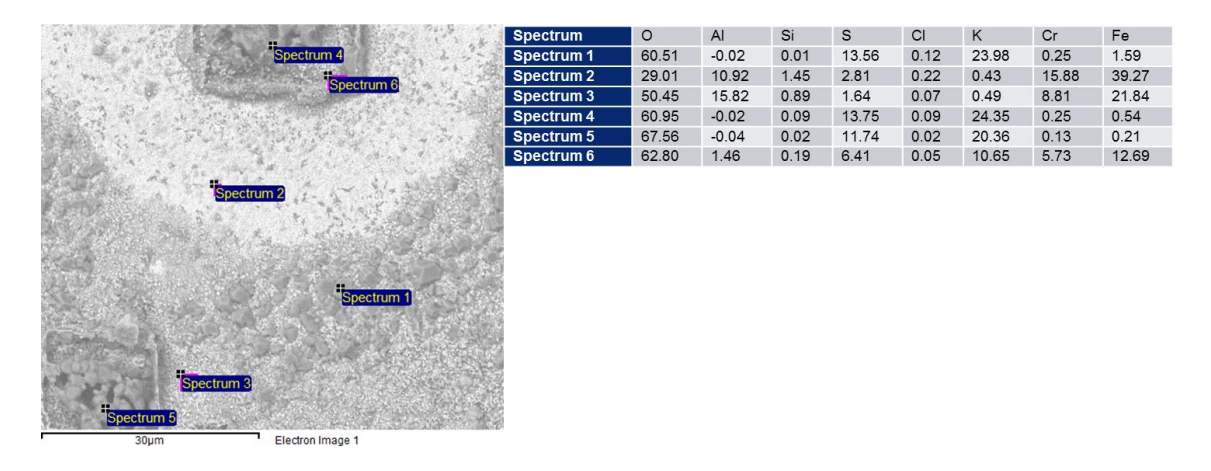
Figure 26. SEM image and EDX analyses of Kanthal[®] APMT after 72 h exposure at 600°C in $5\% O_2 + 40\% H_2O + 300$ ppm $SO_2 + KCI$.

Figure 27 shows EDX maps from the surface of Kanthal® APMT after exposure for 168 hours in O_2 + H_2O + SO_2 + KCl environment. There are some KCl particles with thinner oxide products surrounding them. That kind of region is shown in Figure 27. However these regions are fewer than the regions with more oxide products surrounding them, shown in lower left corner in Figure 28. The elemental maps show that K and S are overlapping at the former KCl particles and at the dark base oxide. The elemental composition fairly coincides with K_2SO_4 in these regions shown by EDX analysis (Figure 28). Chlorine is not detected. Alumina is formed at some regions (Figure 28, spectrum 3).



Figur 27. SEM bild och EDX kartor på Kanthal[®] APMT efter 168 timmars exponering vid 600°C i $5\% \text{ O}_2 + 40\% \text{ H}_2\text{O} + 300 \text{ ppm} + \text{KCI}$.

Figure 27. SEM image and EDX maps of Kanthal[®] APMT after 168 h exposure at 600°C in 5 % O₂ + 40 % H₂O + 300 ppm SO₂ + KCl.



Figur 28. SEM bild och EDX analyser på Kanthal[®] APMT efter 168 timmars exponering vid 600°C i 5 % O_2 + 40 % $H_2\text{O}$ + 300 ppm + KCl.

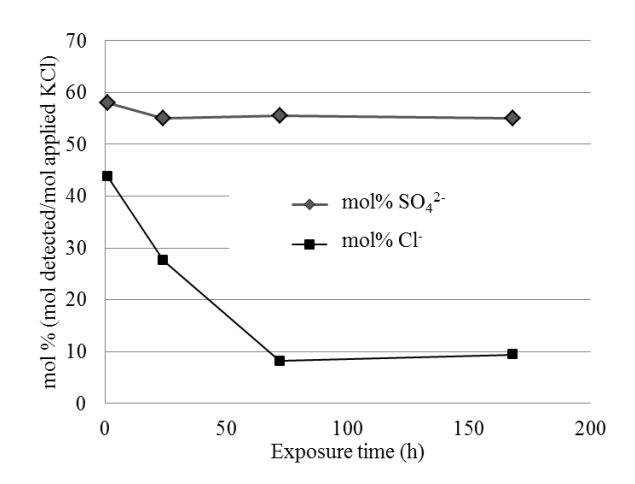
Figure 28. SEM image and EDX analyses of Kanthal[®] APMT after 168 h exposure at 600°C in 5 % O₂ + 40 % H₂O + 300 ppm SO₂ + KCl.

4.2.5 Water-soluble oxide products

Figure 29 shows the levels of soluble oxide products formed on APMT after exposure for 1–168 h of exposure 5% O_2 , 40% H_2O , 300 ppm SO_2 , and KCl. The detected soluble oxide products were $SO_4^{\ 2^-}$ and Cl^- ; the results are presented as mol% (mol detected ion/mol KCl applied).

The levels of $SO_4^{2^-}$ were similar for all exposure times, i.e., approximately 55 mol%. Therefore, assuming that the $SO_4^{2^-}$ corresponds to K_2SO_4 formed from the KCl applied to the sample surface, 55% of the KCl was converted to K_2SO_4 . The mol% Cl^- decreased with exposure time, being about 40 mol% after 1 h of exposure and ≤ 10 mol% after 72 h and 168 h of exposure.

The results indicate that sulfates have formed already after 1 hour exposure and are stable during further oxidation. The decline in Cl^- can be a result of Cl leaving the surface or Cl forming un-soluble corrosion products. It can be concluded that the Cl remaining on the surface is present either as unreacted KCl or as the chlorides of Al, Fe or Cr. The absence of $CrO_4^{2^-}$ implies that no K_2CrO_4 has formed.



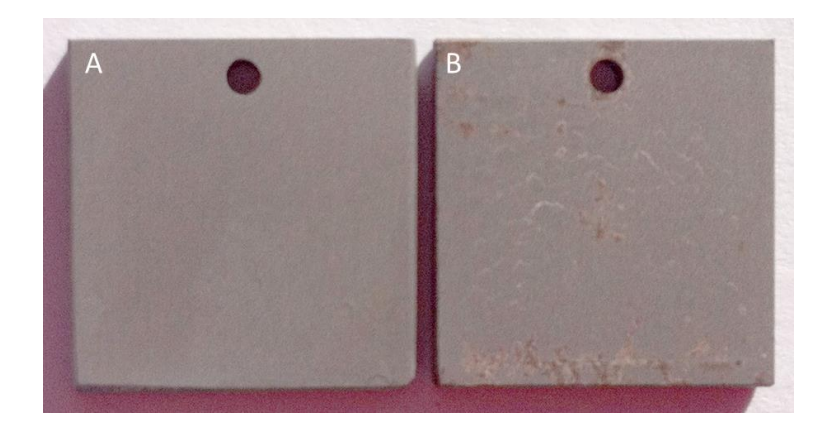
Figur 29. IC analys av de lösliga oxidprodukterna som bilda på Kanthal[®] APMT efter 1 – 168 timmars exponering i 5 % O₂ + 40 % H₂O + 300 ppm SO₂ + KCl.

Figure 29. IC analysis of soluble oxide products formed on alloy APMT after exposure for 1 – 168 h in 5 % O_2 + 40 % H_2O + 300 ppm SO_2 + KCl.

4.3 The effect pre-oxidation in the presence of SO_2 and KCI

4.3.1 Macro apperance

APMT was pre-oxidized at 1100°C for about 1 h and then exposed at 600°C to 5% O_2 , 40% H_2O , 300 ppm SO_2 for 24 h, with KCl being applied to the material surface. The pre-oxidized material exhibited a lusterless grayish surface, whereas the material that was pre-oxidized and thereafter exposed to KCl and SO2 at 600°C exhibited small regions of corrosion and bright curved lines on the grayish lusterless surface (Fig. 30). Therefore, oxide scale produced during the pre-oxidation does not appear to be completely inert in the exposure environment.

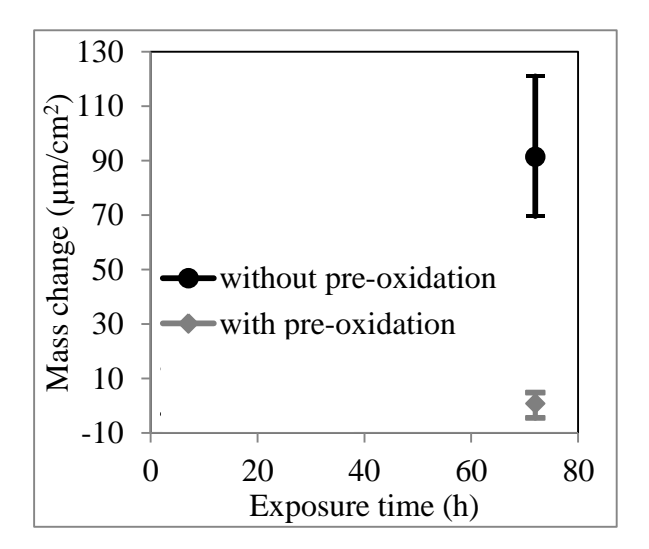


Figur 30. Makrobilder på Kanthal[®] APMT efter A) föroxidering i 1100°C i ca 1h och därefter B) exponering i 72 h vid 600°C i 5 % O₂ + 40 % H₂O + 300 ppm + KCl.

Figure 30. Macro images of Kanthal[®] APMT after A) pre-oxidation at 1100°C for about 1 h and thereafter B9) exposure for 72 h at 600°C in 5 % O_2 + 40 % H_2O + 300 ppm SO_2 + KCl.

4.3.2 Mass gain

The mass change varied between the samples that were subjected to pre-oxidation and subsequent exposure at 600° C for 72 h in the presence of KCl, from -4.5 to +4,9 µg/cm², (Fig. 31). This variance was likely due to spallation as described below. The mass gain in the case without pre-oxidation is 20-fold that observed in this case.

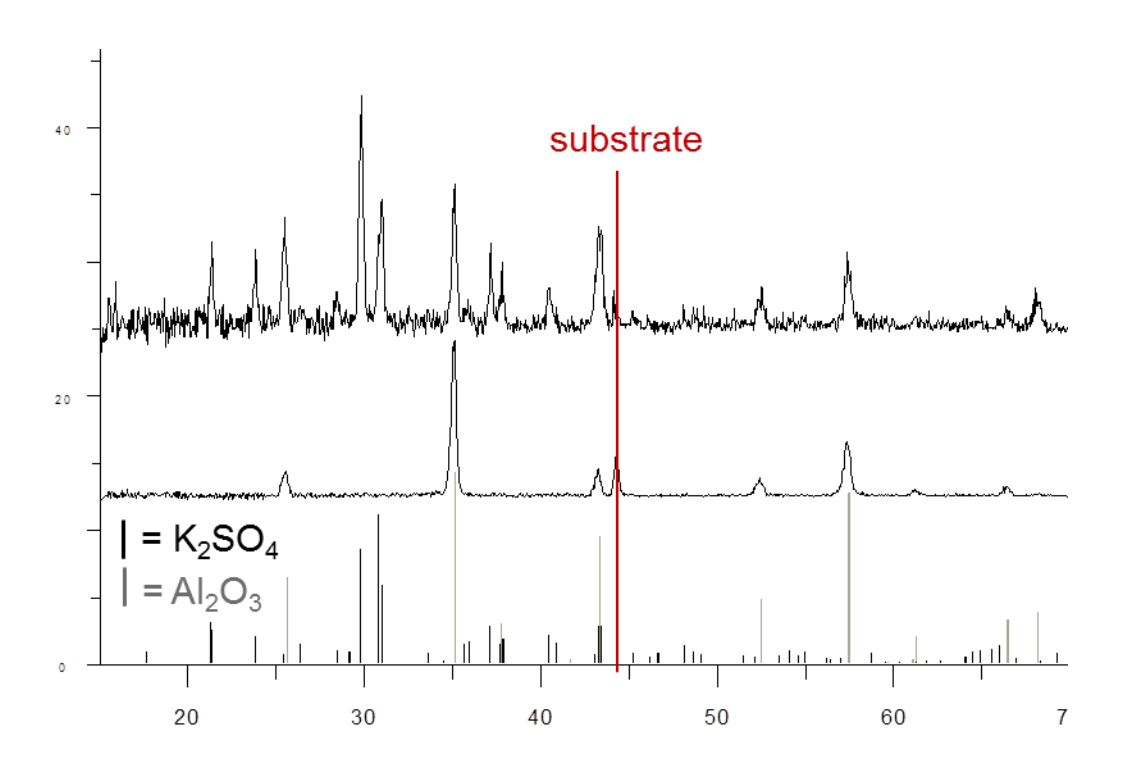


Figur 31. Massökningen för Kanthal[®] APMT med och utan föroxidering efter exponering i 600°C i $5\% \text{ O}_2 + 40\% \text{ H}_2\text{O} + 300 \text{ ppm SO}_2 + \text{KCl.}$

Figure 31. Mass gain for Kanthal[®] APMT with and without pre-oxidation after exposure at 600°C to 5% O₂ with 40% H₂O and 300 ppm SO₂ plus KCl for 72 h.

4.3.3 Crystalline oxide products

The XRD analysis of the pre-oxidized (1100°C, for ~1 h) material showed peaks that corresponded to α -Al $_2$ O $_3$, which indicates that an external α -Al $_2$ O $_3$ scale was established on the material surface (Fig. 32). After exposure at 600°C in the presence of KCl and SO $_2$, α -Al $_2$ O $_3$ was still detected (Fig. 32). Additional peaks that corresponded to K $_2$ SO $_4$ were also detected. No peaks that corresponded to alloy chlorides, chromates or KCl were detected.



Figur 32. Röntgendiffraktogram på Kanthal APMT (underst) föroxidering i 1100°C i ca 1 timma och därefter (överst) exponering i 72 h vid 600°C i 5 % O_2 + 40 % H_2O + 300 ppm + KCl.

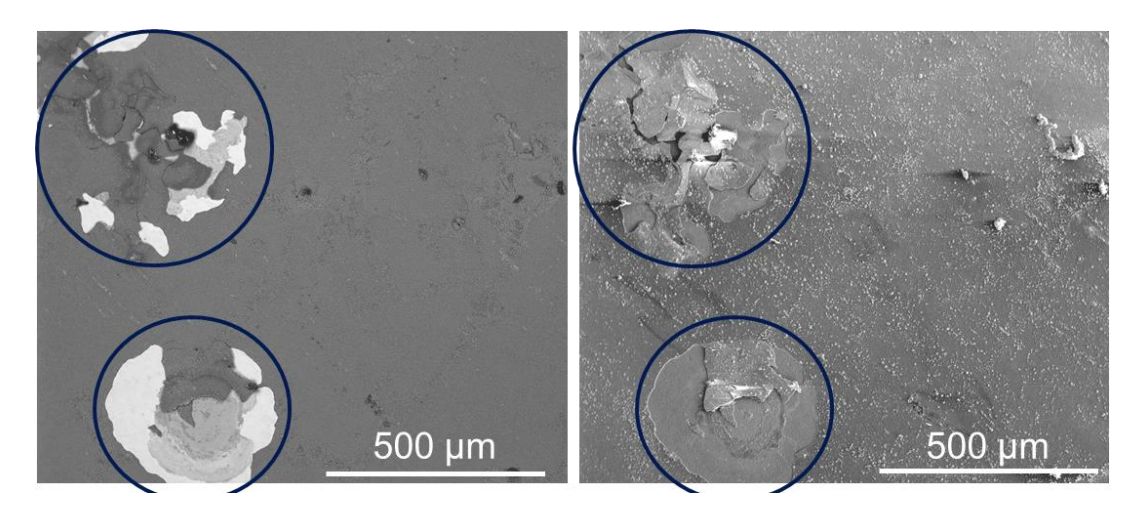
Figure 32. X-ray diffraction of Kanthal APMT after (below) pre-oxidation at 1100°C for about 1 h and thereafter (above) exposure for 72 h at 600°C in 5 % O_2 + 40 % H_2O + 300 ppm SO_2 + KCl.

4.3.4 SEM/EDX

SEM investigation of the alloy after pre-oxidation and subsequent exposure in the presence of KCl and SO_2 revealed some regions where spallation had occurred (indicated with blue circles in Figure 33). However, the spalled regions covered only approximately 4% of the surface, supposing they correspond to the red-brown regions in the macro images (Figure 30). Figure 34 shows the EDX elemental maps of a region that contains some

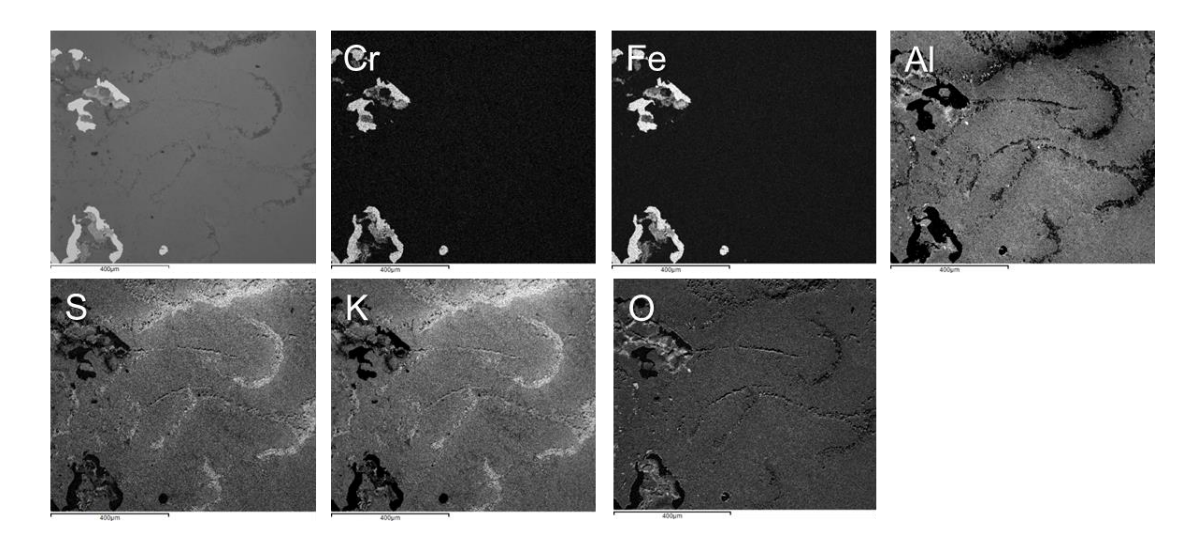
spalled areas, which are bright areas in the Fe and Cr maps and dark areas in

the Al map as a consequence of the lost alumina scale and revealed alloy. The maps also show that the surface is covered in K and S with some thicker banks, likely mimicking the distribution of the applied KCl. In addition, EDX point analysis (Figure 35) shows that the surface is covered with K and S likely corresponding to K_2SO_4 as detected with XRD. Chlorine was not detected.



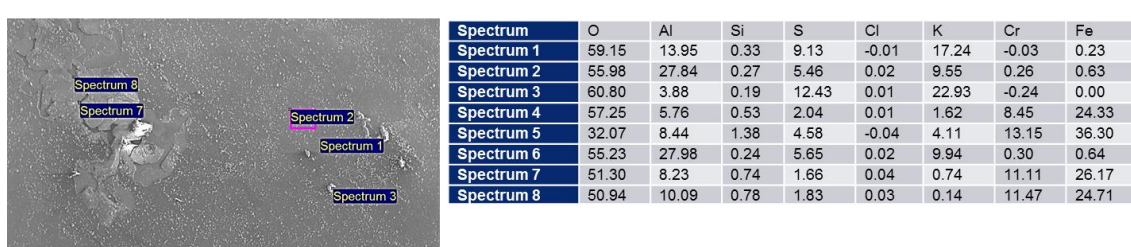
Figur 33. Till vänster; bakåtspridd SEM bild och till höger sekundär SEM bild på Kanthal[®] APMT efter föroxidering i 1100°C i ca 1 timma och därefter exponering i 72 h vid 600°C i 5 % O_2 + 40 % H_2 O + 300 ppm + KCl.

Figure 33. To the left; backscattered SEM image and to the right secondary SEM image of Kanthal[®] APMT after pre-oxidation at 1100°C for about 1 h and thereafter exposure for 72 h at 600°C in 5 % O₂ + 40 % H₂O + 300 ppm SO₂ + KCl.



Figur 34. Till vänster; bakåtspridd SEM bild och element kartor på Kanthal[®] APMT efter föroxidering i 1100°C i ca 1 timma och därefter exponering i 72 h vid 600°C i 5 % O₂ + 40 % H₂O + 300 ppm + KCl.

Figure 34. To the left; backscattered SEM image and element maps of Kanthal® APMT after pre-oxidation at 1100°C for about 1 h and thereafter exposure for 72 h at 600°C



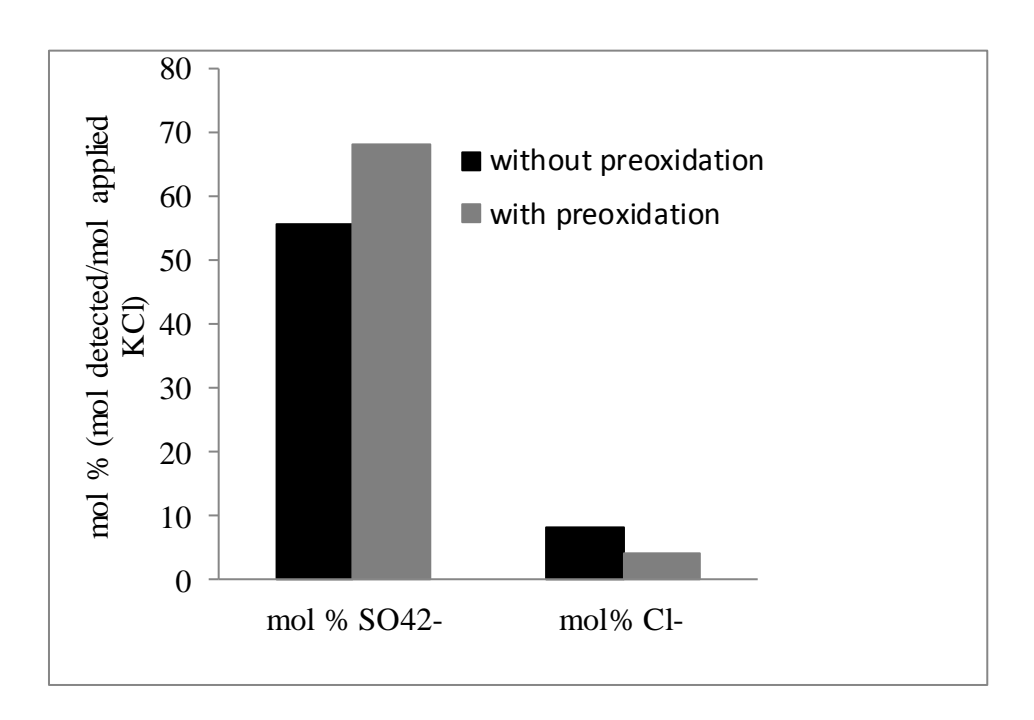
in 5 % O_2 + 40 % H_2O + 300 ppm SO_2 + KCI.

Fiogur 35. Sekundär SEM bild och EDX analyser i atom% på Kanthal[®] APMT efter föroxidering i 1100°C i ca 1 timma och därefter exponering i 72 h vid 600°C i 5 % O₂ + 40 % H₂O + 300 ppm + KCl.

Figure 35. Secondary SEM image and EDX analyses in atom% of Kanthal[®] APMT after preoxidation at 1100°C for about 1 h and thereafter exposure for 72 h at 600°C in 5 % O₂ + 40 % H₂O + 300 ppm SO₂ + KCl.

4.3.5 Water soluble oxide products

The levels of soluble oxide products formed on the APMT alloy after pre-oxidation and subsequent exposure for 72 h at 600°C in the presence of KCl and SO_2 are shown in Figure 36. Interestingly, the levels of $SO_4^{2^-}$ detected on the pre-oxidized sample was almost 70 mol% of the applied KCl which is more than 10 mol% higher than for the sample that did not undergo pre-oxidation. This is likely the result of more KCl being converted to K_2SO_4 due to the absence of other reactions, i.e., alloy chlorination. The levels of Cl in the sample subjected to pre-oxidation were somewhat lower than that in the sample without pre-oxidation.



Fiogur 36. IC analys av vattelösliga oxidprodukter som bildats på APMT med och utan föroxidering, efter exponering under 72 tim i 5 % O₂ med 40 % H₂O och 300 ppm SO₂ plus KCI.

Figure 36. IC analysis of soluble oxide products formed on APMT with and without pre-oxidation, after exposure for 72 h to 5% $\rm O_2$ with 40% $\rm H_2O$ and 300 ppm $\rm SO_2$ plus KCl.

5 Analysis of the results

The corrosivity of alkali chlorides for high-temperature steels is well-known. A way to mitigate this problem in biomass- and waste-fired boilers is to add elemental sulfur to the fuel, thereby increasing the SO_2 concentration in the flue gas, resulting in a substantially reduced corrosion rate for the steel in super heaters, owing to the conversion of reactive alkali chlorides into inert alkali sulfates 6,7 . A possible strategy to decrease even further the corrosion rate is to change from chromia-forming materials to alumina-forming materials, i.e., FeCrAl alloys.

5.1 SO₂

In this investigation it is demonstraited that the oxidation rate of the FeCrAl alloy Kanthal® APMT is very low in the presence of SO2. Comparing these results with the result of previous exposures performed without SO2 shows that the mass gains achieved with and without SO₂ are similar ⁵. Other techniques (AES elemental depth profiles, cross-sectioned SEM imaging, and EDX) reveal similar oxide thicknesses in these two exposure environments. A similar study performed on the chromia-forming material 304L showed that SO₂ has a mitigating effect on the oxidation, with an approximate 5-fold mass decrease in the presence of SO₂ ⁸. The lower oxidation rate was attributed to sulfate being adsorbed at the scale/gas interface, resulting in reduced CrO₂(OH)₂ evaporation and a decrease in rate of reduction of oxygen through blocking of the active sites 8,9. SO₂ did not influence the corrosion rate of APMT in the presence of water vapor. However, it should be noted that the oxidation rate of APMT is very low in this environment and that the mass gain is still 20-times lower than that of 304L after exposure in the same environment

Initially, a layered oxide forms on the APMT, consisting of an inner alumina, a middle chromia, and an outer Fe-rich oxide (see AES and SIMS profiles Figs. 12-15). The Cr- and Fe-containing oxide was detected by XRD as (Fe,Cr)₂O₃. However, no alumina was detected by XRD, indicating a poorly diffracting oxide, i.e., amorphous aluminum oxide. This is also valid for exposures without SO₂ ⁵. Judging from the AES profiles, the oxidation mechanisms for the two oxidation environments, i.e., with and without SO₂, are quite different ⁵. The enrichment for Cr observed in the AES profiles probably represents the original material surface 10. The Al content of the outer layer was lower for the samples exposed in the presence of SO₂ compared with samples exposed in the absence of SO₂, at approximately 5% (24 h) and 10% (168 h) as compared with 18% (24 h) and 30% (168 h), respectively, according to the AES profiles. Thus, the oxidation appears to proceed by inward diffusion of O²⁻ to the oxide metal interface under both exposure conditions. Oxidation also appears to proceed by outward diffusion of Al3+ during oxidation under both exposure conditions, although the rate of diffusion is higher in the atmosphere without SO₂ ⁵. Therefore, SO₂ appears to inhibit the outward growth of the alumina scale. Oxidation of FeCrAl alloys in low-pO2 environments also results

in inhibition of outward growth of the alumina scale; the oxide microstructure contains only elongated grains and lacks the outer equi-axed layer that is observed in high- pO_2 environments 11,12 . Thus, it appears that the presence of SO_2 in the exposure gas results in a decreased oxygen supply for alumina growth. We propose that the sulphate that is being adsorbed at the scale/gas interface (as detected by AES and IC) causes a decrease in the rate of reduction of oxygen by blocking active sites. Judging from the AES profiles, the oxide scale formed in the presence of SO_2 appears somewhat thicker than the one formed without SO_2 . However, the mass gain curves shows that there is no significant difference between the two atmospheres, but the variation is quite large. Thus, the difference in scale thickness is attributed to variations in scale thicknesses and not to a different oxide growth mechanism.

The enrichment of S in the oxide scale, situated between the alumina scale and the area of Cr enrichment (Fig. 15), may be the result of either the initial oxidation, which traps the S in the scale, or S diffusing inwards as the oxidation proceeds. It is suggested that the absorbed sulfate on the surface is reduced by electrons provided by the oxidation of aluminium. The sulfite ions formed is then transported through parts of the oxide scale, along grain boundaries, to the Cr_2O_3/Al_2O_3 interface. Interestingly, S was not detected at the oxide/metal interface, as was the case in another investigation performed on a Fe-2.25Cr-1Mo steel in a similar exposure environment ¹³. Thus, it seems as an alumina layer protects the alloy from sulfidation better than an iron-chromium-rich oxide. This is also consistent with indications from other studies ¹⁴.

5.2 SO₂ and KCl

Exposure to oxygen of Kanthal APMT in the presence of SO_2 and KCl increases considerably the oxidation rate, as compared to an environment that lacks KCl. However, comparing the current results with those for the chromia-forming material 304L, the mass gain of APMT is less than half that of 304L 8 . It is also of interest to compare the above outcomes with the results obtained from exposure of APMT in the presence of KCl but without SO_2 , in which case the mass gain is twice as large initially but is in the same range after 168 h exposure 5 .

The large difference in mass resulting from the different exposure atmospheres observed in the present study can be attributed in part to the conversion of the corrosive KCl into the stable K_2SO_4 in the SO_2 -containing atmosphere (see XRD, IC, and SEM/EDX results in Figs. 19, 20, 22, 23, 25, 27 and 29). During oxidation in an environment with SO_2 and KCl, K_2SO_4 forms according to reaction (1):

$$2KCl(s) + SO_2(g) + H_2O(g) + 1/2O_2(g) \rightarrow K_2SO_4(s) + 2HCl(g)$$
 (1)

Assuming that all of the KCl applied to the material reacts according to reaction (1), then the combined mass loss and gain corresponds to 16 μ g/cm². Comparing this value with the values in the mass gain curve (Fig. 18) shows that the real mass gain is significantly higher (~85 μ g). In addition, the

IC results show that about 55% of the KCl has been converted to K_2SO_4 . Thus, reaction (1) can only explain a part of the overall mass gain.

During oxidation without SO_2 but in the presence of KCl, high levels of K_2CrO_4 were found on the surface of the alloy, depleting the oxide scale of Cr and resulting in a less protective oxide 5 . However, during oxidation in the presence of SO_2 and KCl, no chromates or KCl were detected by XRD, IC or EDX. This is in accordance with recent research showing that within 30 min K_2CrO_4 is converted to K_2SO_4 , according to reaction (3), in an environment that contains O_2 , water vapor and 300 ppm SO_2 15 . Thus, if any of the applied KCl reacts according to reaction (2) to form K_2CrO_4 , it is quickly turned into to sulfate. The discrepancy between the amount of applied KCl and the amount of Cl^- plus SO_4^{2-} may be due to the evaporation of KCl, which is known to be significant at $600^{\circ}C$ 5 .

$$8KCI(s) + 4H_2O(g) + 2Cr_2O_3(s) + 3H_2O(g) \rightarrow 4K_2CrO_4(s) + 8HCI(g)$$
 (2)

$$2K_2CrO_4(s) + 2SO_2(g) \rightarrow 2K_2SO_2(s) + Cr_2O_3(s) + 2.5O_2(g)$$
 (3)

In the regions with high level of Fe-rich oxide, chlorine and loosely detached oxide were detected, indicating alloy chlorination with consequent poor adhesion. Alloy chlorination may be due to the presence of of HCl, which is formed in reactions (1) and (2) and interacts with the alloy instead of evaporating. Previous results also indicate that KCl itself may interact with the alloy, to cause alloy chlorination ¹⁶. Exposure to KCl in the absence of SO₂ results in greater chlorination of the alloy in a dry atmosphere, whereby the KCI remains for a longer period on the surface and reaction (2) proceeds more slowly ⁵. This suggests that corrosion of APMT in the presence of SO₂, KCl, H₂O, and O₂ is mainly due to alloy chlorination, whereas in the presence of KCl, H₂O, and O₂ corrosion is mainly due to K₂CrO₄ formation and to some extent, alloy chlorination. Alloy chlorination leads to weak adhesion of the oxide scale and eventual spallation, which results in rapid oxidation of the uncovered base material. The formation of K₂CrO₄ causes Cr depletion of the oxide scale, leading to poor protection and rapid oxidation of the material. The combined effect of K₂CrO₄ formation and alloy chlorination obviously results in a faster oxidation rate than alloy chlorination alone.

The chlorination process likely involves an electrochemical mechanism, in accordance with Wagner's mechanism for external oxide growth on a metal 17 , whereby the oxidant (e.g., O_2) is reduced at the scale/gas interface, while the metal is oxidized at the scale/metal interface, the two electrodes being connected by electronic and ionic currents, as described by:

$$1/2 O_2 + 2e^- \rightarrow 0^{2^-}$$
 (4)
Me $\rightarrow Me^{2^+} + 2e^-$

In the case of electrochemical chlorination of an alumina-forming alloy by KCl in the presence of SO_2 and O_2 , the cathodic process on the scale surface should generate "free" chloride ions at the surface and incorporate potassium in a stable form. In the present study, the analysis of the scale surface

showed that KCl was consumed and K₂SO₄ formed. Therefore the following set of reactions is suggested to take place:

Scale surface:
$$2KCl(s) + SO_3(g) + 2e^- + O_2(g) \rightarrow K_2SO_4(s) + 2Cl^-(s)$$

Scale/alloy interface: Fe(s) \rightarrow Fe³⁺ + 3e⁻ Cr(s) \rightarrow Cr³⁺ + 3e⁻

 $Al(s) \rightarrow Al^{3+} + 3e^{-}$

The sum reaction becomes (for the case of Fe oxidation):

$$2KCl(s) + SO_3(g) + Fe(s) + 0.5O_2(g) \rightarrow K_2SO_4(s) + FeCl_2(s)$$
 $\Delta G^{\circ}_{900K} = -538 \text{ kJ/mol}$ (5)

After 24 h of oxidation, the species $K_3(Fe,Cr,Al)(SO_4)_3$ was detected (see XRD and SEM/EDX results, Figs. 19 and 23) as predicted by reaction (6):

$$(Fe,Cr,Al)_2O_3(s) + 6SO_2(g) + 6KCl(s) + 3H_2O(g) + 3O_2(g) \rightarrow (6)_2V_3(Fe,Cr,Al)(SO_4)_3(s) + 6HCl(g)$$

 $K_3(Fe,Cr,Al)(SO_4)_3$ was detected only after 24 h of oxidation, and it was consumed before 72 h of oxidation. It is proposed that this compound reacted further according to reaction (7). The occurrence of $K_3(Fe,Cr,Al)(SO_4)_3$ likely varies between samples, supported by the varying corrosion attack between samples, (see error bars in the mass gain curve).

$$2K_3(Fe,Cr,Al)(SO_4)_3(s) + 3H_2O(g) \rightarrow$$
 (7)
 $(Fe,Cr,Al)_2O_3(s) + 3K_2SO_4(s) + 3H_2SO_4(g)$

5.3 The effect of pre-oxidation in the presence of SO₂ and KCl

Pre-oxidation of APMT resulted in the establishment of an external protective α -Al₂O₃ scale (Figure 31). Subsequent exposure of the alloy at 600°C in the presence of KCl and SO₂ resulted in the formation of K₂SO₄, (see XRD, IC and SEM/EDX results in Figs. 31, 33, and 35). The K₂SO₄ likely formed according to reaction (1) as was the case without the protective scale. Some of the applied KCl appeared to have evaporated, which would explain the IC results, where about 75% of the applied KCl could be accounted for by summing the detected levels of SO₄²⁻ and Cl⁻.

A small proportion of the surface of the alloy showed regions in which the protective scale had been spalled off (Figs. 32 and 33). After spallation, the alumina scale is probably not re-healed owing to the low rate of Al diffusion at the exposure temperature used. The spallation may be the result of cracks that originate from the cooling between exposures and that are due to thermal expansion mismatch. Another possible explanation is that alloy chlorination generates decreased adherence and spallation. About 5% of the Cl⁻ was detected with IC. The origin of these Cl⁻ is not known, since no

chlorides were detected by EDX or XRD. However the chlorine most likely originated from alloy chlorination, supported by the spallation process. Chlorination is suggested to proceed through reaction (5), with the same electrochemical mechanism as described above for the material without preoxidation. Interestingly, the level of Cl⁻ detected by IC was doubled in the samples without pre-oxidation, indicating that a faster chlorination rate occurs without pre-oxidation. Taken together, these results propose Kanthal APMT as an interesting candidate for combustion plant components, especially from a corrosion point of view.

It is important to note that these results are obtained from laboratory exposures in an environment mimicking that of a boiler containing about 300 ppm SO_2 in the flue gas. The results obtained after probe exposure at 600°C of FeCrAl material in Händelö P14 (KME 507) showed a larger material loss with than without pre-oxidation. However, that boiler does not have a sulphur recycling system. That is, Händelö P14 has relatively low SO_2 content in the flue gas. Thus, the conversion of the corrosive KCl into stable K_2SO_4 is not as pronounced as in our laboratory investigation. The higher amount of the corrosive KCl may be one factor that increases the spallation of the alumina. It may be noted that the flue gas composition in the real boiler is much more complex than in the laboratory environment. That is, other unknown factors may also play a role in the different behaviours of the FeCrAl material exposed in KME 519 (laboratory exposures) and 507 (field exposures).

6 Conclusions

The oxidation of the FeCrAl material Kanthal APMT was investigated at 600 °C in the environments of O_2 with H_2O and SO_2 and O_2 with H_2O , SO_2 and KCl, and compared with the oxidation behaviors in the environments of O_2 with H_2O and O_2 with O_2 with O_2 with O_2 with O_3 wi

For SO₂

- The oxidation rate of Kanthal APMT is very low in the presence of SO₂.
- Initially, a layered oxide forms with an inner alumina, a middle chromia, and an outer Fe-rich oxide.
- The outward alumina growth appears to be suppressed in the presence of SO₂.
- Sulfur enrichment is observed on the surface and between the alumina scale and the zone of Cr enrichment.

For SO₂ plus KCl

- Exposing the material to oxygen in the presence of SO₂ and KCl increases considerably the oxidation rate, as compared with an environment without KCl.
- More than half of the applied KCl is converted to stable K_2SO_4 on the surface of the material during the exposure. $K_3(Fe,Cr,Al)(SO_4)_3$ is also found on the material surface albeit only after 24 h of exposure. $K_3(Fe,Cr,Al)(SO_4)_3$ is likely converted to K_2SO_4 with time.
- Cl is present where the corrosion has started, implying alloy chlorination.

For pre-oxidation with subsequent exposure to SO₂ and+ KCl

- Pre-oxidation of Kanthal APMT results in the establishment of an external protective α -Al₂O₃ scale.
- Subsequent exposure at 600° C in the presence of KCl and SO_2 results in the formation of K_2SO_4 and the evaporation of KCl.
- A small proportion of the alloy surface shows regions where the protective scale has been spalled off.
- The spallation may be a result off cracks that appear due to thermal expansion mismatch and/or alloy chlorination.
- After spallation, the alumina scale is probably not re-healed owing to the low rate of Al diffusion at the exposure temperature used.

In summarize; The alumina-forming FeCrAl material Kanthal APMT is not completely inert to KCl in an oxidizing SO_2 -containing atmosphere at 600°C. However, the corrosion rate is significantly lower than that of the commonly used chromia-forming alloy, 304L. Pre-oxidation decreases the corrosion rate even further, making Kanthal APMT a promising candidate material for combustion plant components, particularly from a corrosion point of view.

7 Goal fulfilment

The project has investigated the influence of SO_2+H_2O and $SO_2+KCI+H_2O$ on the corrosion of a FeCrAl alloy through laboratory exposures. The influence of pre-oxidation before exposure to the above environment has also been examined. The material was thereafter analyzed by a range of different analytical techniques which has provided new knowledge about the corrosion in these environments.

Thus, the project has performed all planned activities successfully.

8 Suggestions for future research work

The limitations and usability of FeCrAl alloys in biomass- and waste- fired boilers are still far from being fully understood. There are several issues that should be addressed by future work;

- Further investigate the influence of environments that resemble the corrosive environment in real boilers on FeCrAl materials with and without pre-oxidation.
- Further investigate the temperature range in which FeCrAl materials perform satisfying in environments that resemble the corrosive environment in real boilers and in real boilers
- Investigate performance of different alumina forming coatings/compound tubes in biomass and waste fired boiler environments at different temperatures
- Investigate the effect of applying an external alumina coating, not by pre-oxidizing which affects the composition of the substrate material.

9 Literature references

- (1) Jonsson, B.; Berglund, R.; Magnusson, J.; Henning, P.; Hattestrand, M. High temperature properties of a new powder metallurgical FeCrAl alloy. High Temperature Corrosion and Protection of Materials 6, Prt 1 and 2, Proceedings 2004, 461-464, 455-462.
- (2) H., J.; F., L.; J.-E., S.; M., H.; L.-G., J. The formation of oxide scale on FeCrAl at 900°C in dry O2 and O2 + 40% H2O. *Proceedings Electro Chemical Society, High Temperature Corrosion and Materials Chemistry V* **2005**, 56-66.
- (3) Liu, F.; Götlind, H.; Svensson, J.-E.; Johansson, L.-G.; Halvarsson, M. Early stages of the oxidation of a FeCrAIRE alloy (Kanthal AF) at 900 °C: A detailed microstructural investigation. *Corrosion Science* **2008**, *50*, 2272-2281.
- (4) Israelsson, N.; Engkvist, J.; Hellström, K.; Halvarsson, M.; Svensson, J.-E.; Johansson, L.-G. KCl-induced corrosion of a FeCrAl alloy at 600°C in O2 + H2O environment The effect of pre-oxidation. *Oxidation of Metals* **2013**, *Submitted*.
- (5) Israelsson, N. High Temperature Corrosion of FeCrAl alloys Chalmer University of Technology, 2013.
- (6) Pettersson, J.; Pettersson, C.; Folkeson, N.; Johansson, L. G.; Skog, E.; Svensson, J. E. The influence of sulphur additions on the corrosive environment in a waste-fired CFB boiler. *High-Temperature Oxidation and Corrosion 2005* **2006**, *522-523*, 563-570.
- (7) Folkeson, N.; Pettersson, J.; Pettersson, C.; Johansson, L. G.; Skog, E.; Andersson, B. A.; Enestam, S.; Tuiremo, J.; Jonasson, A.; Heikne, B.; Svensson, J. E. Fireside corrosion of stainless and low alloyed steels in a waste-fired CFB boiler; The effect of adding sulphur to the fuel. High Temperature Corrosion and Protection of Materials 7, Pts 1 and 2 2008, 595-598, 289-297.
- (8) Karlsson, S.; Pettersson, J.; Svensson, J. E.; Johansson, L. G. KCl-Induced High Temperature Corrosion of the Austenitic Stainless Steel 304L-The Influence of SO2. *Mater Sci Forum* **2011**, 696, 224-229.
- (9) Jardnas, A.; Svensson, J. E.; Johansson, L. G. Influence of SO2 on the oxidation of 304L steel in O-2+40%H2O at 600 degrees C. Oxidation of Metals 2008, 69, 249-263.
- (10) Liu, F.; Josefsson, H.; Svensson, J. E.; Johansson, L. G.; Halvarsson, M. TEM investigation of the oxide scales formed on a FeCrAIRE alloy (Kanthal AF) at 900 degrees C in dry O-2 and O-2 with 40% H2O. *Mater High Temp* **2005**, *22*, 521-526.
- (11) Huntz, A. M.; Marechal, L.; Lesage, B.; Molins, R. Oxidation of alumina forming materials. *Elec Soc S* **2003**, *2003*, 18-32.
- (12) Young, D. J.; Naumenko, D.; Niewolak, L.; Wessel, E.; Singheiser, L.; Quadakkers, W. J. Oxidation kinetics of Y-doped FeCrAl-alloys in low and high pO(2) gases. *Mater Corros* **2010**, *61*, 838-844.
- (13) Jardnas, A.; Svensson, J. E.; Johansson, L. G. The inhibitive effect of traces of SO2 on the oxidation of iron. *Oxidation of Metals* **2003**, *60*, 427-445.

- (14) Kofstad, P. High Temperature Corrosion. 1988.
- (15) S., K. Submitted to Energy and Fuels **2013**.
- (16) Israelsson, N.; Hellström, K.; Svensson, J.-E.; Johansson, L.-G. KCl-induced corrosion of the FeCrAl alloy Kanthal AF at 600°C and the effect of H₂O. Oxidation of Metals **2013**, submitted.
- (17) P., K.: *High Temperature Corrosion*; Applied Science publishers Ltd.: London and New York: Elsiver, 1988.

10 Publications

List of publications resulting from the project

The combined effect of sulfur dioxide and potassium chloride on the oxidation of a FeCrAl alloy

K. Hellström, J. Engkvist, P. Malmberg, Yuo Cao, Mats Norell and J.-E. Svensson Manuscript

Appendices



SVENSKA ELFÖRETAGENS FORSKNINGS- OCH UTVECKLINGS - ELFORSK - AB

Elforsk AB, 101 53 Stockholm. Besöksadress: Olof Palmes Gata 31 Telefon: 08-677 25 30, Telefax: 08-677 25 35 www.elforsk.se